NASA/TM-1999-208745

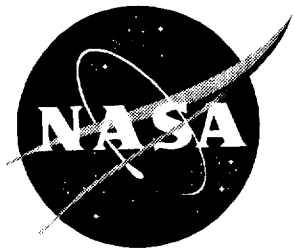

A Parametric Study of Accelerations of an Airplane Due to a Wake Vortex System

Eric C. Stewart
Langley Research Center, Hampton, Virginia

National Aeronautics and
Space Administration

Langley Research Center
Hampton, Virginia 23681-2199

May 1999

Available from:

NASA Center for AeroSpace Information (CASI)
7121 Standard Drive
Hanover, MD 21076-1320
(301) 621-0390

National Technical Information Service (NTIS)
5285 Port Royal Road
Springfield, VA 22161-2171
(703) 605-6000

Abstract

A study was conducted using strip theory to systematically investigate the effects of progressively more complete descriptions of the interaction of an airplane with a wake vortex system. The emphasis was in roll-dominant, parallel, vortex encounters. That is, the simulated airplane's longitudinal axis was nearly parallel to the rotation axis of the vortex system for most of the results presented. The study began with a drag-less rectangular wing in the flow field of a single vortex and progressed to a complete airplane with aerodynamic surfaces possessing taper, sweep, dihedral, and stalling and immersed in the flow field of a vortex pair in ground effect. The effects of the pitch, roll, and yaw attitudes of the airplane on the calculated accelerations were also investigated. The airplane had the nominal characteristics of a Boeing 757, and the vortex flow field had the nominal characteristics of the wake of a Boeing 767. The Burnham-Hallock model of a vortex flow field was used throughout the study. The data are presented mainly in terms of contours of equal acceleration in a two-dimensional area centered on the vortex pair and having dimensions of 300 feet by 300 feet.

Introduction

For years many different people have calculated or simulated the interactions of airplanes with the wake of other airplanes, references 1–5. Analytical models of vortex flow fields lend themselves to a variety of approaches ranging from purely analytical closed-form solutions to more complex computer simulations. Since there is no standardized approach, each study has its own set of simplifying assumptions. As a result interpreting the results of different studies and simulations is often confusing. In addition, some of the more complex simulations take large computer resources that may be prohibitive for real-time piloted simulations. For example, a portable math model with a minimum of input parameters is needed for airline training simulators. That is, the model must capture the dominant vortex encounter effects, but must be simple enough so that it can be adapted to a wide variety of airplanes and airplane simulators with a minimum of effort.

The present study compares the theoretical effects of some of the major simplifications that can be made to a math model of a vortex encounter. The study starts with one of the simplest situations—a rectangular wing in a single, isolated vortex field with the longitudinal axis of the airplane aligned with the rotation axis of the vortex. Strip theory is used to calculate the three angular and three linear accelerations produced by the isolated vortex flow field. The accelerations are calculated at a matrix of points in the two-dimensional area around the flow field. A popular plotting program is then used to calculate contours of constant acceleration in the two-dimensional area. Additional contours are calculated for increasingly more complex geometries and orientations of the airplane relative to the axis of the vortex system. By comparing the different contours the effects of the different parameters can be visualized.

Symbols

A acceleration, ft^2/sec

Area area of surface, ft^2

b	span of aerodynamic surface, ft
c	chord of aerodynamic surface, ft
c_d	drag coefficient of incremental surface area
c_r	chord of surface at the root, ft
c_l	lift coefficient of incremental surface element
$c_{l,o}$	lift coefficient at assumed flight condition
$c_{l,\alpha}$	lift curve slope for incremental surface element, per radian
F	force, lbf
I_{xx}	moment of inertia about the x axis, slug-ft^2
I_{yy}	moment of inertia about y axis, slug-ft^2
I_{zz}	moment of inertia about z axis, slug-ft^2
j	index for aerodynamics surfaces (right wing, left wing, right horizontal tail, left horizontal tail, and vertical tail)
k	index for incremental surface elements
l_y	semi-span of surface (positive for starboard surfaces), ft
ΔL	lift on incremental surface element, lbf
M	rotational moment, ft-lbf
N	number of incremental surface elements
$\bar{q}$ [	dynamic pressure, lbf/ft^2
$\bar{q}\varepsilon$	dynamic pressure at incremental surface area corrected for sweep, lbf/ft^2
r_r	radius from center of right vortex to three-quarter chord point of incremental surface element, ft
r_l	radius from left vortex to three-quarter chord point of incremental surface element, ft
$r_{c,r}$	radius of vortex core of right vortex, ft
$r_{c,l}$	radius of vortex core of left vortex, ft
u,v,w	velocity components of vortex flow field in x,y,z direction in earth axis system, ft/sec
V	airspeed, ft/sec

$V_{\varepsilon.tot}$ airspeed at three-quarter chord point perpendicular to sweep line, ft/sec

W weight of airplane, lbf

X longitudinal axis, figure 1

x x location, ft

$\bar{x}$ x location of the quarter chord of the mean aerodynamic chord measured from apex of wing panels, ft

x_{b4} x location of one-quarter chord incremental surface area, ft

x_{so} x location of surface axis system relative to body axis system, ft

x_{s4} x location of quarter-chord of incremental surface element in surface coordinate system, ft

Y lateral axis, figure 1

y y location, ft

$\bar{y}$ y location of mean aerodynamic chord, ft

Z vertical axis, figure 1

z z location, ft

α angle of attack, degrees or radian

α_{stall} stall angle of attack of incremental surface element, radian

β_o nominal angle of sideslip, degrees

ε angle of rotation about z axis of surface axis system (related to sweep angle), radian

Λ sweep angle of quarter-chord line of surface, degrees

λ taper ratio (tip chord divided by root chord)

ψ,θ,ϕ Euler angles of body axis system relative to earth axis system, degrees

$\ddot{\phi}$ roll acceleration, deg/sec^2

$\ddot{\psi}$ yaw acceleration, deg/sec^2

$\ddot{\theta}$ pitch acceleration, deg/sec^2

Γ_r circulation of right vortex, ft^2/sec

Γ_l circulation of left vortex, ft^2/sec

ρ density of air, .002378 slug/ft^3

η rotation about x axis of surface axis system relative to body axis system (related to dihedral), degrees

Δ Area incremental surface area, ft^2

Subscripts:

b body axis system

cg center of gravity

e earth axis system

g generator airplane

h horizontal tail

l left vortex

o zero or trim condition in the absence of the vortex flow field

r right vortex

s aerodynamic surface axis system

h horizontal tail

v vertical tail

w wing

x,y,z x,y,z direction

ε rotation about z axis (related to sweep)

Operator:

• derivative with respect to time

Math Model

The situation studied is sketched in Figure 1. The vortex system is assumed to extend in a straight line to infinity in either direction so that the problem is two-dimensional. Besides the earth axis system, whose origin is located between the two vortices, the other axis systems of interest are the airplane body axis system, and five aerodynamic surface axis systems. The five aerodynamic surface axis systems are used to model the right and left wing panels, the right and left horizontal tail panels, and the vertical tail panel. The body axis system is located at an arbitrary (y_{cg}, and z_{cg}) position and angular orientation relative to the earth axis system. The orientation is specified by the standard airplane yaw, pitch, and roll

Euler angles (ψ,θ,ϕ). The five aerodynamic surface axis systems are located at arbitrary x_{so} positions and rotation angles η (about the x-axis) relative to the airplane body axis system. The following equations, which are used for the wing and tail surfaces, are written in general terms for a planar aerodynamic surface with sweep, taper, and dihedral. No fuselage is modeled, and it is assumed that the aerodynamic surfaces originate at the centerline of the airplane. Each surface is broken up into N spanwise incremental areas (N = 100 for each of the wing surfaces, and N = 25 for the tail surfaces). The angle of attack and sideslip at the three-quarter-chord point of each incremental area is calculated independent of its neighbors while the forces are assumed to act at the quarter-chord point of each incremental area. The steps in the program can be summarized as follows:

Step 1. Specify velocity of follower airplane

$$V = 269 \text{ fps}$$

Step 2. Define coordinates of points in the aerodynamic surface coordinate system.

A. Three-quarter chord points

$$c_r = \frac{2\text{Area}}{(1+\lambda)|l_y|}$$

$$y_s = l_y \frac{(k-.5)}{N} \qquad k = 1,2,3\ldots N$$

$$x_s = -\frac{3}{4}c_r - |y_s| \left(\tan\Lambda + \frac{\frac{1}{2}(\lambda-1)c_r}{|l_y|} \right)$$

$$z_s = 0$$

B. One-quarter chord points.

$$x_{s4} = -\frac{1}{4} c_r - |y_s| \tan\Lambda$$

Step 3. Define the aerodynamic center of a swept and tapered wing.

$$\bar{y} = \frac{b}{2} \frac{(1+2\lambda)}{3(1+\lambda)}$$

$$\bar{x} = -\frac{1}{4}(c_r - \bar{y} \tan\Lambda)$$

Step 4. Place the origin of the body axis system on the wing centerline at one-quarter of the wing mean aerodynamic chord aft of the wing apex. Transform the surface axis coordinates to body axis system. These surface and body axis systems differ in the x coordinate of the origin and a single rotation angle, η, about the x-axis ($|\eta|$ = dihedral angle for the wing and horizontal tail).

$$x_b = x_s + x_{so}$$

$$x_{b4} = x_{s4} + x_{so}$$

$$\begin{bmatrix} y_b \\ z_b \end{bmatrix} = \begin{bmatrix} \cos(\eta) & -\sin(\eta) \\ \sin(\eta) & \cos(\eta) \end{bmatrix} \begin{bmatrix} y_s \\ z_s \end{bmatrix}$$

Step 5. Transform from body axis coordinate system to earth axis system.

$$\begin{bmatrix} x_e \\ y_e \\ z_e \end{bmatrix} = [c(\psi, \theta, \phi)] \begin{bmatrix} x_b \\ y_b \\ z_b \end{bmatrix} + \begin{bmatrix} x_{cg} \\ y_{cg} \\ z_{cg} \end{bmatrix}$$

where

$$[c(\psi, \theta, \phi)] = \begin{bmatrix} \{\cos(\theta)\cos(\psi)\} & \{\sin\phi\sin\theta\cos\psi & \{\cos\phi\sin\theta\cos\psi \\ & -\cos\phi\sin\psi\} & +\sin\phi\sin\psi\} \\ \{\cos(\theta)\cos(\psi)\} & \{\sin\phi\sin\theta\sin\psi & \{\cos(\phi)\sin(\theta)\sin(\psi) \\ & +\cos\phi\cos\psi\} & -\sin(\phi)\cos(\psi)\} \\ \{-\sin(\theta)\} & \{\sin(\phi)\cos(\theta)\} & \{\cos(\phi)\cos(\theta)\} \end{bmatrix}$$

Step 6. Calculate velocity components due to vortex system in earth axis system. (This vortex model was developed by Burnham and Hallock, reference 6)

$$u = 0$$

$$v = \frac{1}{2\pi}\left[\Gamma_r \frac{(z_e - z_r)}{\left(r_{c,r}^2 + r_r^2\right)} - \Gamma_l \frac{(z_e - z_l)}{\left(r_{c,l}^2 + r_l^2\right)}\right]$$

$$w = \frac{1}{2\pi}\left[\Gamma_l \frac{(y_e - y_l)}{\left(r_{c,l}^2 + r_l^2\right)} - \Gamma_l \frac{(y_e - y_r)}{\left(r_{c,r}^2 + r_r^2\right)}\right]$$

$\Gamma_l = \Gamma_r = \dfrac{4W_g}{\pi\rho V_g b_g}$ where the subscript g is for generator airplane

$$z_l = z_r = 0$$

$$y_r = -y_l = \frac{b_g \pi}{0}$$

Note: When ground effect is investigated, two counter-rotating image vortices are placed equidistant below the ground plane.

Step 7. Calculate nominal velocity components (without the vortex-induced velocities) in body axis system.

$$\alpha_o = c_{l,o}/c_{l,\alpha}$$
$$\beta_o = 0.0$$

$$\begin{bmatrix} u_b \\ v_b \\ w_b \end{bmatrix} = \begin{bmatrix} V\cos(\beta_o)\cos(\alpha_o) \\ V\sin(\beta_o) \\ V\cos(\beta_o)\sin(\alpha_o) \end{bmatrix}$$

Step 8. Calculate total velocity components (including the vortex-induced velocities) in earth axis system.

$$\begin{bmatrix} \dot{x}_e \\ \dot{y}_e \\ \dot{z}_e \end{bmatrix} = [c(\psi, \theta, \phi)] \begin{bmatrix} u_b \\ v_b \\ w_b \end{bmatrix} - \begin{bmatrix} u \\ v \\ w \end{bmatrix}$$

Step 9. Transform the total velocity components to the aerodynamic surface coordinate system.

$$\begin{bmatrix} u_s \\ v_s \\ w_s \end{bmatrix} = [t(\psi, \theta, \phi, \eta)] \begin{bmatrix} \dot{x}_e \\ \dot{y}_e \\ \dot{z}_e \end{bmatrix}$$

where

$$[t(\psi, \theta, \phi, \eta)] = \begin{bmatrix} 1 & 0 & 0 \\ 0 & \cos(\eta) & \sin(\eta) \\ 0 & -\sin(\eta) & \cos(\eta) \end{bmatrix} [c(\psi, \theta, \phi)]^T$$

Step 10. Calculate the velocity components perpendicular to the sweep line

$$\begin{bmatrix} u_\varepsilon \\ v_\varepsilon \\ w_\varepsilon \end{bmatrix} = \begin{bmatrix} \cos(\varepsilon) & \sin(\varepsilon) & 0 \\ -\sin(\varepsilon) & \cos(\varepsilon) & 0 \\ 0 & 0 & 1 \end{bmatrix} \begin{bmatrix} u_s \\ v_s \\ w_s \end{bmatrix}$$

where $\varepsilon = \Lambda$ for right wing and tail panels, $\varepsilon = -\Lambda$ left wing and tail panels.

Step 11. Calculate angle of attack and velocity perpendicular to sweep line

$$V_{\varepsilon,tot} = \sqrt{w_\varepsilon^2 + u_\varepsilon^2}$$

$$\alpha = \tan^{-1}(w_\varepsilon / u_\varepsilon)$$

Step 12. Calculate local lift and drag coefficients of each incremental surface area.

$$c_l = c_{l_\alpha}\alpha \qquad \text{for } |\alpha| \le \alpha_{stall}$$

$$c_l = c_{l_\alpha}\alpha_{stall}\text{SIGN}(\alpha) \qquad \text{for} |\alpha| \le \alpha_{stall}$$

$$c_d = .017 + k \cdot c_l^2$$

where

$$k = [(2)(\text{Area})] / \left[(.85)\pi(2|l_y|)^2\right]$$

Step 13. Calculate lift and drag of each incremental surface area.

$$\Delta\text{Area} = \frac{|l_y|}{N} c_r \left[1 + \frac{(\lambda - 1)|y_s|}{|l_y|}\right]$$

$$\bar{q}_\varepsilon = \frac{1}{2}\rho V_{\varepsilon,tot}^2$$

$$\Delta L = \bar{q}_\varepsilon \cdot \Delta\text{Area} \cdot c_l$$

$$\Delta D = \bar{q}_\varepsilon \cdot \Delta\text{Area} \cdot c_d$$

Step 14. Transform lift and drag to surface axis system from stability axis system.

$$\begin{bmatrix} F_{x,s} \\ F_{y,s} \\ F_{z,s} \end{bmatrix} = \begin{bmatrix} \cos(\alpha) & 0 & -\sin(\alpha) \\ 0 & 1 & 0 \\ \sin(\alpha) & 0 & \cos(\alpha) \end{bmatrix} \begin{bmatrix} -\Delta D \\ 0 \\ -\Delta L \end{bmatrix}$$

Step 15. Transform forces to body axis from surface axis system.

$$\begin{bmatrix} F_x \\ F_y \\ F_z \end{bmatrix} = \begin{bmatrix} 1 & 0 & 0 \\ 0 & \cos(\eta) & -\sin(\eta) \\ 0 & \sin(\eta) & \cos(\eta) \end{bmatrix} \begin{bmatrix} F_{x,s} \\ F_{y,s} \\ F_{z,s} \end{bmatrix}$$

Step 16. Calculate body axis moments.

$$\begin{bmatrix} M_x \\ M_y \\ M_z \end{bmatrix} = \begin{bmatrix} y_b \cdot F_z - z_b \cdot F_y \\ z_b \cdot F_x - xb4 \cdot F_z \\ -y_b \cdot F_x + xb4 \cdot F_y \end{bmatrix}$$

Step 17. Sum incremental forces and moments for the j_{th} aerodynamic surface and convert to accelerations.

$$\begin{bmatrix} (A_x)_j \\ (A_y)_j \\ (A_z)_j \end{bmatrix} = \begin{bmatrix} \sum_{i=1}^{N} F_x/W \\ \sum_{i=1}^{N} F_y/W \\ \sum_{i=1}^{N} F_z/W \end{bmatrix}$$

$$\begin{bmatrix} \ddot{\phi}_j \\ \ddot{\theta}_j \\ \ddot{\psi}_j \end{bmatrix} = \begin{bmatrix} \sum_{i=1}^{N} M_x/I_{xx} \\ \sum_{i=1}^{N} M_y/I_{yy} \\ \sum_{i=1}^{N} M_z/I_{zz} \end{bmatrix}$$

Step 18. Sum over the five aerodynamic surfaces to produce total acceleration on airplane.

$$\begin{bmatrix} A_x \\ A_y \\ A_z \end{bmatrix} = \begin{bmatrix} \sum_{j=1}^{5} (A_x)_j \\ \sum_{j=1}^{5} (A_y)_j \\ \sum_{j=1}^{5} (A_z)_j \end{bmatrix} - \begin{bmatrix} A_{x,o} \\ A_{y,o} \\ A_{z,o} \end{bmatrix}$$

where j=right wing, left wing, right horizontal tail, left horizontal tail, vertical tail, and $A_{x,o}$, $A_{y,o}$, $A_{z,o}$ are the accelerations with the vortex absent.

$$\begin{bmatrix} \ddot{\phi} \\ \ddot{\theta} \\ \ddot{\psi} \end{bmatrix} = \begin{bmatrix} \sum_{j=1}^{5} \ddot{\phi}_j \\ \sum_{j=1}^{5} \ddot{\theta}_j \\ \sum_{j=1}^{5} \ddot{\psi}_j \end{bmatrix} - \begin{bmatrix} \ddot{\phi}_o \\ \ddot{\theta}_o \\ \ddot{\psi}_o \end{bmatrix}$$

where j=right wing, left wing, right horizontal tail, left horizontal tail, vertical tail, and $\ddot{\phi}_o$, $\ddot{\theta}_o$, $\ddot{\psi}_o$ are the accelerations with the vortex absent.

Procedure

A Fortran program was written for the preceding equations. The six accelerations were calculated at 2-ft intervals over a 300-ft by 300-ft area in the y-z plane of the earth axis system. The output of the program was written to a file that was then used as input to a popular plotting program to produce the desired contour plots.

The wake vortex flow field was calculated using the equations in Step 6 of the math model section using the constants shown in table I.

Table I. Constants for generator airplane (patterned after Boeing 767)

V_g, ft/sec	b_g, ft	W_g, lbf	$r_{c,r} = r_{c,l}$, ft
280	156.1	285,000	2

The calculations were conducted in order of increasing complexity of the math model. That is, the first calculations are for a single vortex and a simple rectangular wing. Succeeding calculations add a trim lift coefficient, drag, taper, dihedral, sweep, stalling, and then vertical and horizontal tail surfaces to represent the complete airplane. The values of these features for the complete airplane are given in table II.

Table II. Characteristics of aerodynamic surfaces for complete follower airplane (patterned after Boeing 757)

Surface	Area, ft^2	$c_{l,o}$	l_y, ft	λ	η, degrees	ε, degrees	N	x_{so}, ft
Lt wing	1951/2	1.0	−124.5/2	.23	5	−25	100	$-\bar{x}$
Rt wing	1951/2	1.0	124.5/2	.23	−5	25	100	$-\bar{x}$
Lt h. tail	677/2	0.0	−49.9/2	.40	8	−31	25	$-76 + \bar{x}$
Rt. h. tail	677/2	0.0	49.9/2	.40	−8	31	25	$-76 + \bar{x}$
V. tail	495	0.0	22.4	.38	−90	35	25	$-60 + \bar{x}$

Because this study concentrated on variations geometric and aerodynamic properties of the math model, other important parameters were held fixed. For example, one of the most powerful parameter affecting the accelerations is the section lift curve slope, $c_{l,\alpha}$. However, for this study it was assumed to have a constant value of 5.00 per radian for all five aerodynamic surfaces. This value is reasonable for this class of airplanes. In addition, all calculations are made for one set of mass characteristics and flight condition of the follower airplane, table III.

Table III. Constants for follower airplane (patterned after Boeing 757)

V, ft/sec	β_o, degrees	W, lbf	I_{xx}, slug-ft^2	I_{yy}, slug-ft^2	I_{zz}, slug-ft^2
269	0	168,000	2,300,000	3,000,000	4,000,000

The plots are presented in the sequence shown in table IV showing the incremental effect of the next parameter on the previous configuration. The "Vortex" column indicates whether a single (right) vortex, a double vortex, or four vortices were used for a particular figure. In all cases the circulation strength was calculated based on the characteristics in table I which produced a circulation strength of 4160 ft^2/sec using a density of .002378 slug/ft^3 for air. The "X's" in the other columns indicate that the appropriate features were active. In figure 5, for example, the trim lift coefficient, the drag components, the dihedral, sweep, the surface areas of the vertical and horizontal tail surfaces, and the roll, yaw, and pitch attitude angles were all set equal to zero. In addition, the taper ratio was set equal to 1.0 and the stall angle of attack was set equal to a large number (10^5 radians). Thus, the configuration presented in figure 5 is a simple rectangular wing with its axis perfectly aligned to the axis of a double vortex. An "X" in one of the last three columns indicates that the designated attitude angle was incremented +20° from the nominal attitude that was aligned with the vortex axis. For most of the figure sequence, the pattern is to add a single new factor to each successive figure. Thus, the effect of each factor can be determined by comparing any two sequential figures. Of course, such a procedure will not expose possible interactions of the factors with each other.

Table IV. Summary of characteristics used in plotted figures

Figure	Vortex	Wing	α_o	Drag	Taper	Dihedral	Sweep	Stall	V. tail	H. tail	Roll	Yaw	Pitch
2	single												
3	single	X											
4	double												
5	double	X											
6	double	X	X										
7	double	X	X	X									
8	double	X	X	X	X								
9	double	X	X	X	X	X							
10	double	X	X	X	X	X	X						
11	double	X	X	X	X	X	X	X					
12	double	X	X	X	X	X	X	X	X				
13	double	X	X	X	X	X	X	X	X	X			
14	double	X	X	X	X	X	X	X	X	X	X		
15	double	X	X	X	X	X	X	X	X	X	X	X	
16	double	X	X	X	X	X	X	X	X	X	X	X	X
17	double	X	X	X	X	X	X	X	X	X	Unlimited		
18	double	X	X	X	X	X	X	X	X	X		90°	
19	four*												
20	four*	X	X	X	X	X	X	X	X	X			

*Simulates a double vortex near the ground.

The numerical levels of the acceleration contour lines are the same for all the acceleration contour figures in order to make the comparisons easier. That is, all the angular acceleration (roll, yaw, and pitch) contours have possible numerical levels of (0, ±10, ±20 degrees/sec^2, - - -). Likewise, all the linear acceleration (z, y, and x) contours have possible numerical levels of (0, ±0.1, ±0.2 g's, - - -). Therefore, the relative magnitude and extent of the acceleration fields can be determined by noting the number of contour lines and their spacing.

Results

The vortex flow field of an isolated right vortex produced by the Burnham-Hallock model with a core radius of 2 ft is shown in figure 2. The flow is symmetric about the center of the vortex which is located at y_{cg} = 61.2 ft, z_{cg} = 0. The velocities near the core are much larger than those at a distance from the center.

Acceleration contours for a planar, rectangular wing in the vortex flow field of figure 2 are shown in figure 3. The rolling acceleration contours are more complex than the basic flow field because different parts of the wing are experiencing different flow conditions at the same time. The largest accelerations are in roll and the z-axis as would be expected for a rectangular wing. Both accelerations change sign as the wing transverses the flow field in the y direction.

The vortex flow field of two counter-rotating vortices of the same type as shown in figure 2 is presented in figure 4. Although the vortices are rotating in opposite directions, there is very little cancellation of velocities except at distances of over approximately 100 feet from either vortex center. That is, the 5-ft/sec contour in figure 2 extends to a larger distance than does the corresponding contour in figure 4. In addition, the total areas enclosed by the 10 ft/sec and higher valued contours about twice as large for the two vortex system as that for the single vortex system.

The next fourteen figures show accelerations produced by the system of two counter-rotating vortices described in figure 4. For example, the accelerations for a planar rectangular wing in the two-vortex system are shown in figure 5. Because the wing is planar, the dominant accelerations are again in the roll and z-axes. However, the accelerations are greater and cover a larger area than those for a single vortex shown in figure 3. The acceleration contours are more complex also in that there are four areas of alternating sign in the roll acceleration as the airplane transverses the vortices in the y direction. Thus, it appears that for vortices of the same strength, a two-vortex system may be more hazardous than a single vortex system for this span ratio. It has been suggested previously that a single vortex system might be more hazardous than a vortex pair. It was reasoned that if the wing of the follower airplane spanned counter-rotating vortices their effects would tend to cancel. In this case, the span of follower airplane was almost exactly the same as the separation of the two vortices, and there appears to be very little cancellation.

Adding the effect of a non-zero initial angle of attack (corresponding to $c_{l,o}$ = 1.0), to the calculations produces a 11.46 degree rotation of the lift vector relative to the body axes. In order to maintain a parallel encounter, the pitch attitude was also rotated 11.46 degrees. These small rotations have very little effect on the accelerations as can be seen by comparing figure 6 to figure 5. The two dominant accelerations, roll and z, are virtually identical. There are some small differences in the yaw and x accelerations, but the levels are still relatively small. It should be remembered that only the incremental effects of the vortex on the accelerations are show here. For example, offsets such as the 1g z acceleration due the non-zero lift coefficient have been removed by the zero terms as shown in step 18 of the math model section.

Adding the effect of drag, likewise, had no significant effect on any of the accelerations, figure 7. Again it should be remembered that only the effect of the incremental drag due to the vortex is shown in figure 7.

Adding taper (taper ratio = .23) to the planar rectangular wing, figure 8, reduces average roll acceleration as expected. With less wing area at the wing tips, the moment in roll is reduced. However, the z acceleration is relatively unaffected.

Adding dihedral (5 degrees) to the tapered wing of figure 8 has very little effect on any of the accelerations, figure 9. The contours for the pitch and y acceleration change appearance, but the acceleration levels are still small compared to the roll and z acceleration respectively.

Adding sweep (sweep angle = 25 degrees) to the wing of figure 9 slightly reduces the roll and z accelerations, see figure 10. This is due to the fact that sweep reduces the component of the free-stream velocity normal to the wing's quarter chord line. Only the normal component of the velocity is used to calculate the dynamic pressure at each incremental wing area.

Adding localized stalling (stall angle of attack = 15 degrees) to the wing for the regions of high vortex velocities had surprisingly little effect on the overall acceleration contours, figure 11. Near the center of the vortices the contours of roll acceleration and z accelerations have new small areas of high inflection. However, the area enclosed by each contour level is virtually the same as without stalling.

Adding the vertical tail to the previous wing had very little effect on the z accelerations, figure 12. The roll acceleration was increased slightly, and there is some inflection in the ±20 degree roll acceleration contours below the centers of the vortices. These areas of inflection are due to the stalling of the vertical tail in the high velocity areas near the vortex cores. Adding the vertical tail increased the yaw and y accelerations significantly from the wing-alone values. However, their magnitudes are much less than those for roll and z because of the smaller size of the vertical tail compared to the wing.

Adding the horizontal tail to the previous configuration had a bigger effect than the vertical tail, figure 13. The added surface area of the horizontal tail increased both the roll and z acceleration. The effect on the yaw and y acceleration was minimal, but the maximum pitch acceleration contour was increased to over 40 deg/sec^2. The x acceleration was also increased.

Rolling the previous (complete airplane) configuration to an attitude of 20 degrees, distorted all the acceleration contours, figure 14. The maximum contour levels are not greatly affected. However, the contours are not simply rotated 20 degrees as might be expected.

Adding 20 degrees of yaw, and then 20 degrees of pitch, to the previous roll attitude, further distorts the contours, see figures 15 and 16 respectively. These results clearly demonstrate the complexity of a vortex encounter in which the attitude as well as the trajectory of the airplane through the vortex field affects the accelerations experienced.

The contours of roll angle for zero rolling moment are presented in figure 17. These contours indicate the positive equilibrium roll angles for a simulated airplane if it were restrained in all axes except roll (1 degree of freedom). The five other accelerations are not equal to zero so a 6 degree of freedom simulated airplane is not in equilibrium on these contours. However, since the response in the roll axis is the dominant response, this figure gives insight into the expected response. That is, the figure demonstrates that outside the immediate areas around the vortices, the simulated airplane will not tend to roll indefinitely as might be thought from the previously presented figures. If the simulated airplane is

located over the left vortex (e.g. at $y_{cg} = -75$, $z_{cg} = -100$) and has an initial roll attitude of zero, it will have positive roll acceleration, see figure 13. However, figure 17 indicates that after it rolls to 60 degrees, the roll acceleration would be equal to zero. It should be noted that only positive values are shown for the contours in figure 17. There are also negative roll angles at which the roll acceleration is zero.

The accelerations for a perpendicular vortex encounter are shown in figure 18. In this case the rolling, yawing, and y accelerations are zero because of the symmetry of the airplane. The other accelerations are similar in magnitude and regional extent to those for the parallel encounter, compare to figure 13. However, there are small regions around the vortex cores where there are much higher accelerations. These higher accelerations are due to the fact that a larger area of the wing is exposed to the high core velocities when there is a perpendicular encounter than for a parallel encounter. The fact that these regions are so small means that the probability of hitting them is much smaller. In addition, the time the airplane experiences these accelerations is very short compared to a parallel encounter so that, in general, the perpendicular encounter causes a smaller upset. However, there is a possibility of structural damage if the airplane penetrates the small areas of high core velocities.

The final figures, figures 19 and 20, explore the effect of a ground plane in the vicinity of the vortex pair. The flow field is modified by the presence of the ground so that there is only flow tangential to the ground ($z_{cg} = 150$ ft) and no flow perpendicular or through the ground plane. However, the velocities near the ground are small compared to those near the centers of the vortex. The acceleration contours are, therefore, practically the same as those for the corresponding conditions away from the ground (figure 13). The only real differences are near the ground where the accelerations are small in the first place. Of course, if the vortices were closer to the ground (for example, 50 ft), these differences would be larger.

Concluding Remarks

A systematic investigation has been made of a math model of the interaction of an airplane with a wake vortex system. The math model was based on strip theory with arbitrary geometric characteristics of the aerodynamic surfaces. The wake vortex flow field of both a single vortex and a vortex pair was modeled using the Burnham-Hallock model with the nominal wake characteristics of a B767 airplane. The six rigid body accelerations of a B757-like airplane were calculated for increasing levels of complexity of the math model. Starting with a planar rectangular wing at zero lift coefficient and no drag, a non-zero lift coefficient, drag, taper, dihedral, sweep, stalling effects, a vertical tail, and a horizontal tail were added. The effects of changes in the airplane attitude about a nominal parallel orientation were also investigated. The following observations were made.

(1) The effects of the single vortex field extended to larger distances from the vortex core than did the effects of a counter-rotating vortex pair. However, near the cores the effects of the vortex pair were greater and covered a larger area. In addition, the acceleration contours for the vortex pair were more complicated with more sign reversals. Thus, it appears that a vortex pair has a greater hazard potential than a single vortex.

(2) The dominant accelerations were in the roll and z-axis although significant yawing, pitching, and lateral accelerations were calculated when the vertical and horizontal tails were added to the model. The longitudinal acceleration was not a major factor.

(3) A non-zero lift coefficient, drag, wing dihedral and localized stalling had negligible effects on the accelerations compared to taper ratio and sweep.

(4) The effect of twenty-degree attitude changes in all three axes significantly distorted all the acceleration contours.

(5) The z and pitch accelerations f or a perpendicular encounter were generally comparable to those for a parallel encounter except for small areas of much larger accelerations around the vortex cores. The rolling, yawing, and lateral accelerations, however, were zero due to the symmetry of the airplane.

(6) The effect of the presence of a ground plane at 150 ft below the vortex was minimal except when the encountering airplane was near the ground.

References

1. Smith, W. G.; and Lazzeroni, F. A.: *Experimental and Theoretical Study of a Rectangular Wing in a Vortical Wake at Low Speed.* NASA TN D-339, Oct. 1960.

2. McMillan, O. J.; Schwind, R. G.; Nielsen, J.N.; and Dillenius, M.F.E.: Rolling Moments in a Trailing Vortex Flowfield, *J. Aircr.*, May 1978.

3. Hastings, Earl C., Jr.; and Keyser, Gerald L: *Simulation Study of Vortex Encounters by a Twin-Engine, Commercial, Jet Transport Airplane.* NASA TP-1966, Feb. 1982.

4. Rossow, V. J.: Estimate of Loads During Wing-Vortex Interactions by Munk's Transverse-Flow Method. *J. Aircr.*, Jan. 1990.

5. Reimer, Heidi M.; and Vicroy, Dan D.: *A Preliminary Study of Wake Vortex Encounter Hazard Boundary for a 737-100 Airplane.* NASA TM-110223, Apr. 1996.

6. Hallock, J.N.: *Aircraft Wake Vortices: An Assessment of the Curent Situation.* DOT-FAA-RD-90-29, Jan. 1991.

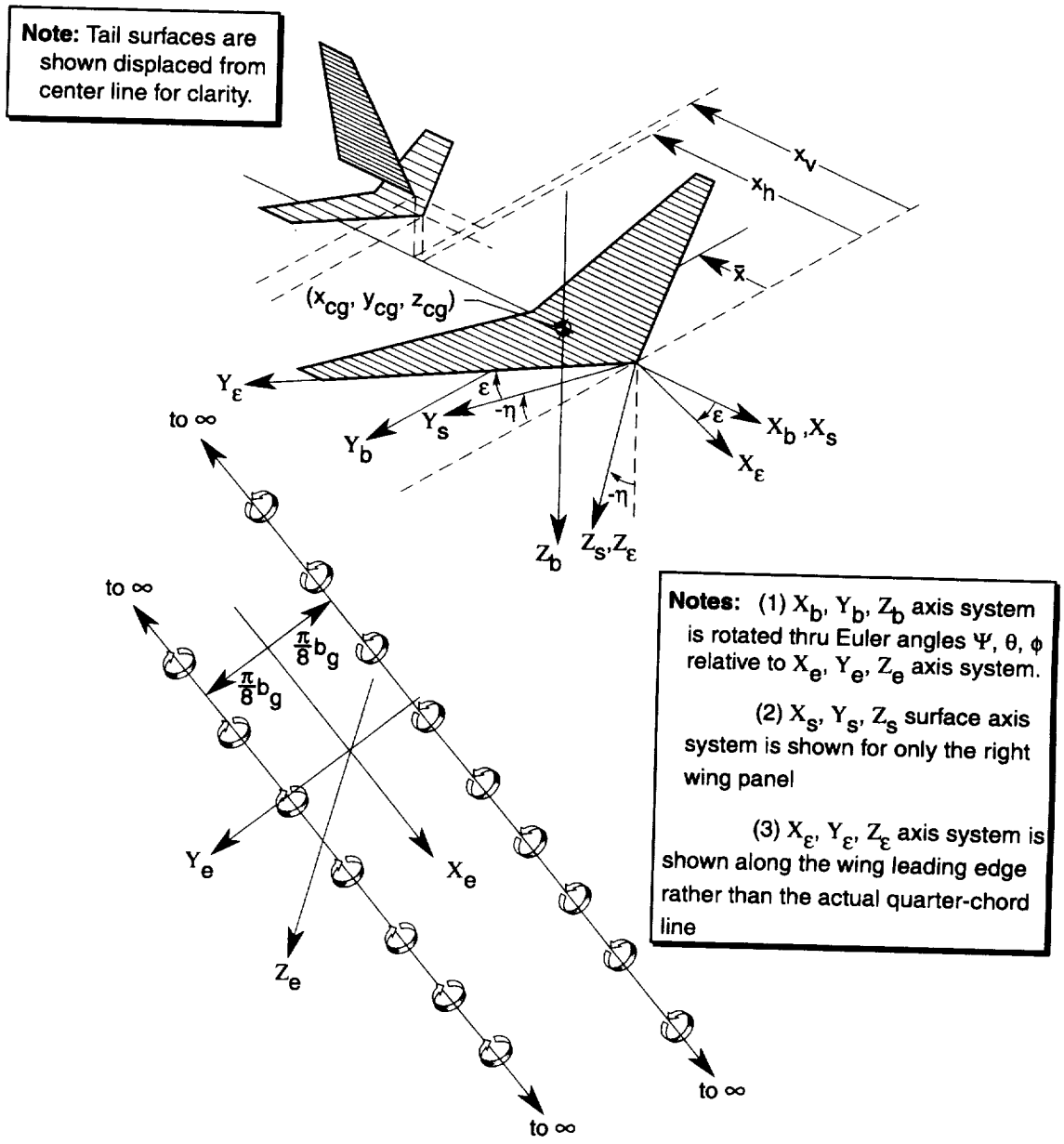

Figure 1a. Axis systems used in study.

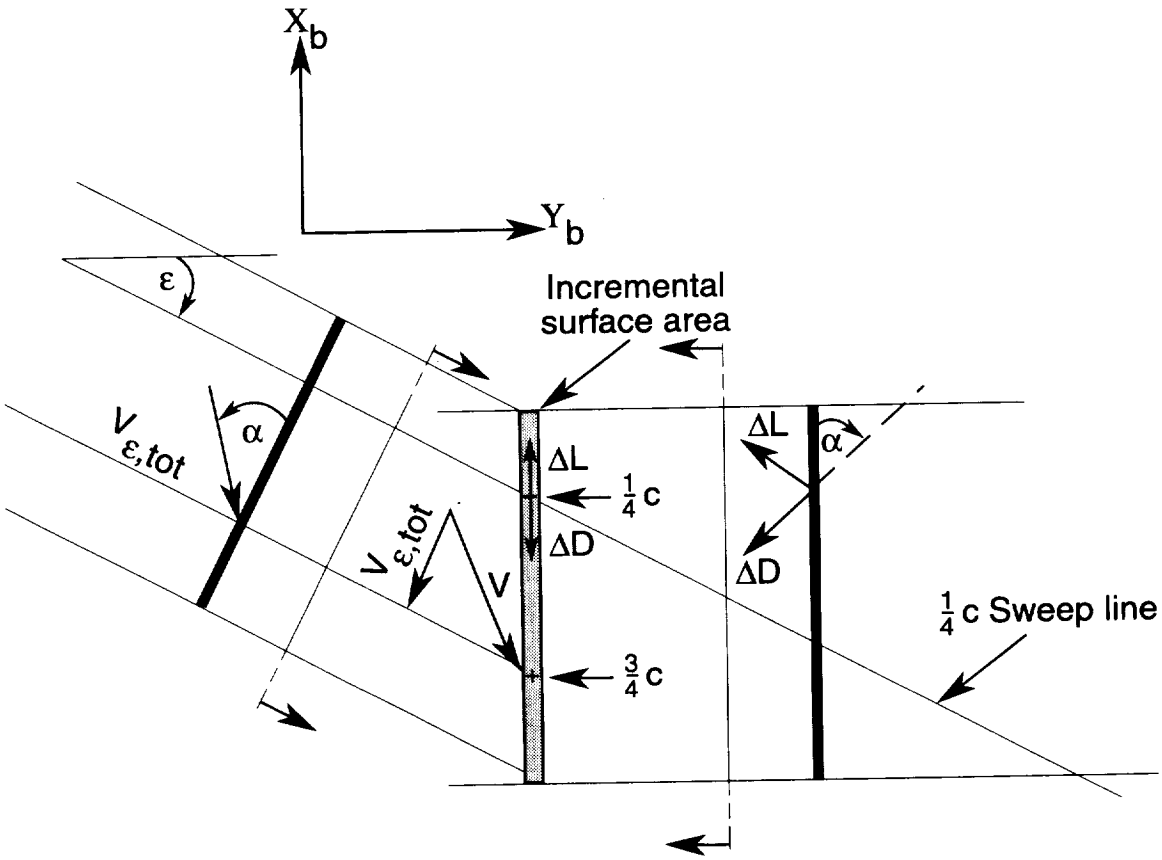

Figure 1b. Detail of geometry of an incremental surface area showing flow angles and aerodynamic forces.

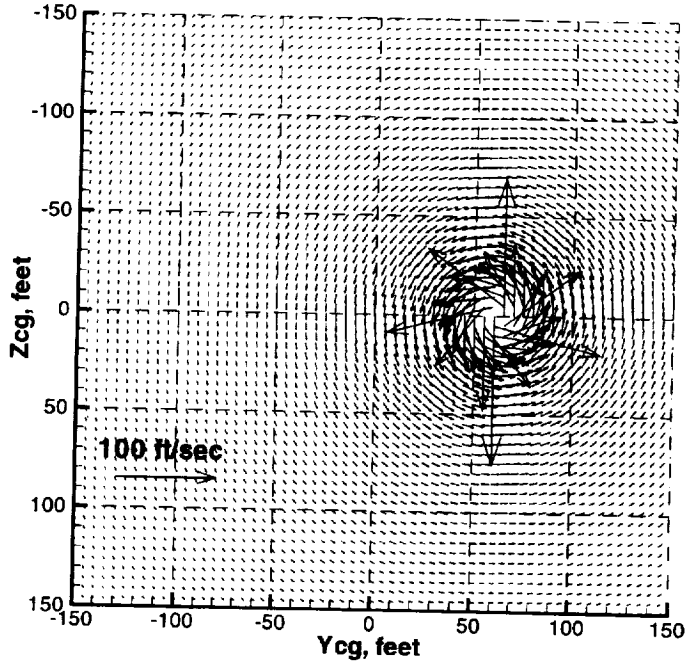

(a) Velocity vector plot.

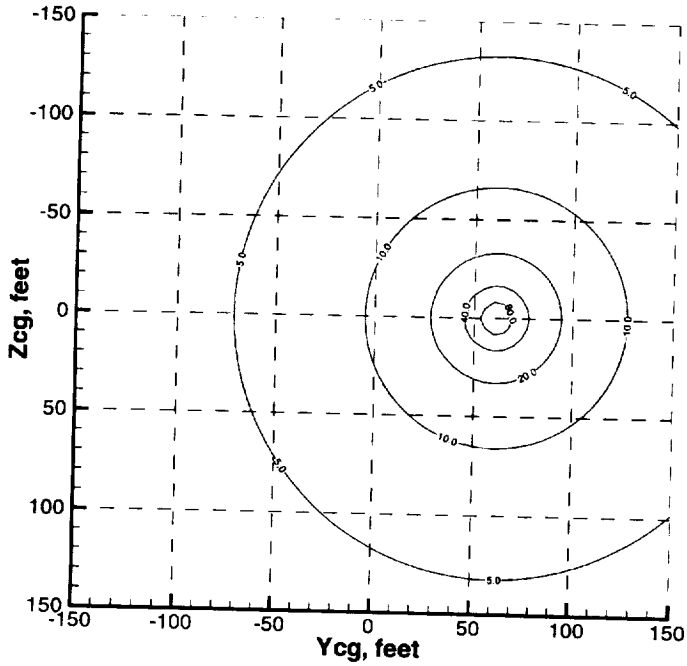

(b) Velocity contour plot

Figure 2. Flow field of a single vortex with a circulation strength of 4160 ft^2/sec.

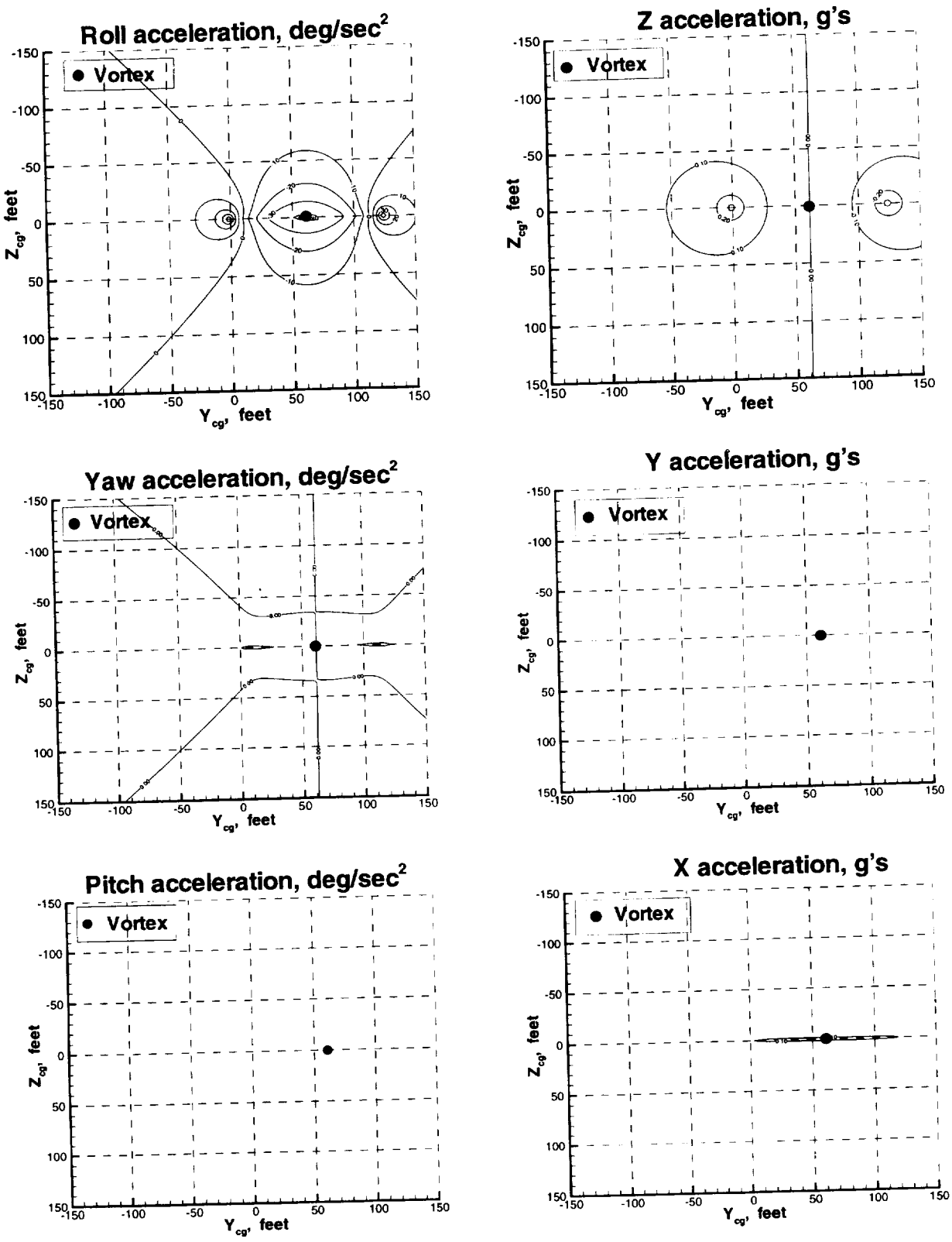

Figure 3. Acceleration contours for rectangular wing in flow field of a single vortex.

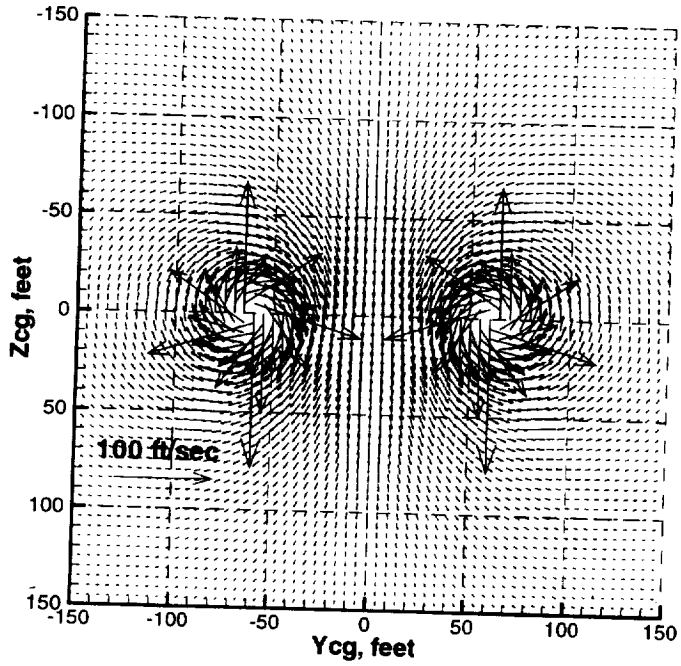

(a) Velocity vector plot.

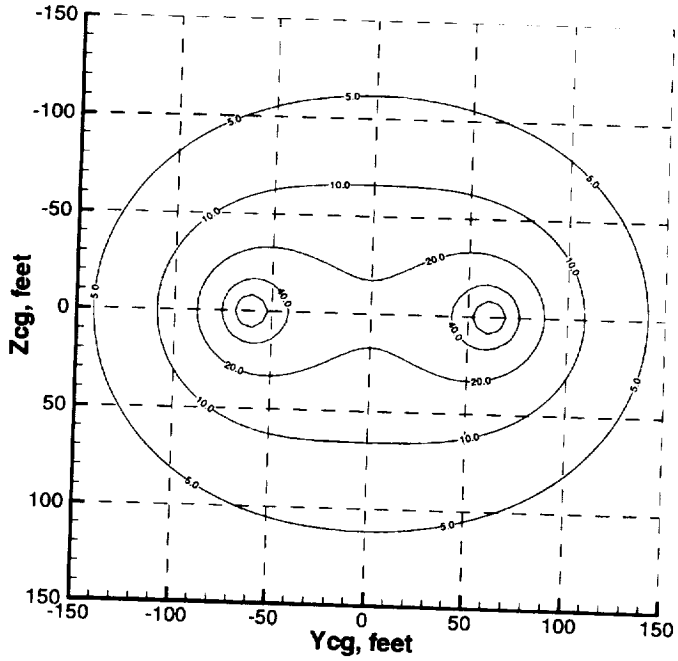

(b) Velocity contour plot.

Figure 4. Total velocity flow field of a vortex pair with a circulation strength of 4160 ft^2/sec.

REPORT DOCUMENTATION PAGE

Form Approved
OMB No. 07704-0188

1. AGENCY USE ONLY *(Leave blank)*	2. REPORT DATE	3. REPORT TYPE AND DATES COVERED
	May 1999	Technical Memorandum

4. TITLE AND SUBTITLE
A Parametric Study of Accelerations of an Airplane Due to a Wake Vortex System

5. FUNDING NUMBERS
WU 538-04-11-12

6. AUTHOR(S)
Eric C. Stewart

7. PERFORMING ORGANIZATION NAME(S) AND ADDRESS(ES)
NASA Langley Research Center
Hampton, VA 23681-2199

8. PERFORMING ORGANIZATION REPORT NUMBER
L-17831

9. SPONSORING/MONITORING AGENCY NAME(S) AND ADDRESS(ES)
National Aeronautics and Space Administration
Washington, DC 20546-0001

10. SPONSORING/MONITORING AGENCY REPORT NUMBER
NASA/TM-1999-208745

11. SUPPLEMENTARY NOTES

12a. DISTRIBUTION/AVAILABILITY STATEMENT
Unclassified–Unlimited
Subject Category 02 Distribution: Standard
Availability: NASA CASI (301) 621-0390

12b. DISTRIBUTION CODE

13. ABSTRACT ***(Maximum 200 words)***

A study was conducted using strip theory to systematically investigate the effects of progressively more complete descriptions of the interaction of an airplane with a wake vortex system. The emphasis was in roll-dominant, parallel, vortex encounters. That is, the simulated airplane's longitudinal axis was nearly parallel to the rotation axis of the vortex system for most of the results presented. The study began with a drag-less rectangular wing in the flow field of a single vortex and progressed to a complete airplane with aerodynamic surfaces possessing taper, sweep, dihedral, and stalling and immersed in the flow field of a vortex pair in ground effect. The effects of the pitch, roll, and yaw attitudes of the airplane on the calculated accelerations were also investigated. The airplane had the nominal characteristics of a Boeing 757, and the vortex flow field had the nominal characteristics of the wake of a Boeing 767. The Burnham-Hallock model of a vortex flow field was used throughout the study. The data are presented mainly in terms of contours of equal acceleration in a two-dimensional area centered on the vortex pair and having dimensions of 300 feet by 300 feet.

14. SUBJECT TERMS	15. NUMBER OF PAGES
Wake vortex, Airplane simulation, Airplane dynamics, Wake vortex encounters	41
	16. PRICE CODE A03

17. SECURITY CLASSIFICATION OF REPORT	18. SECURITY CLASSIFICATION OF THIS PAGE	19. SECURITY CLASSIFICATION OF ABSTRACT	20. LIMITATION OF ABSTRACT
Unclassified	Unclassified	Unclassified	UL

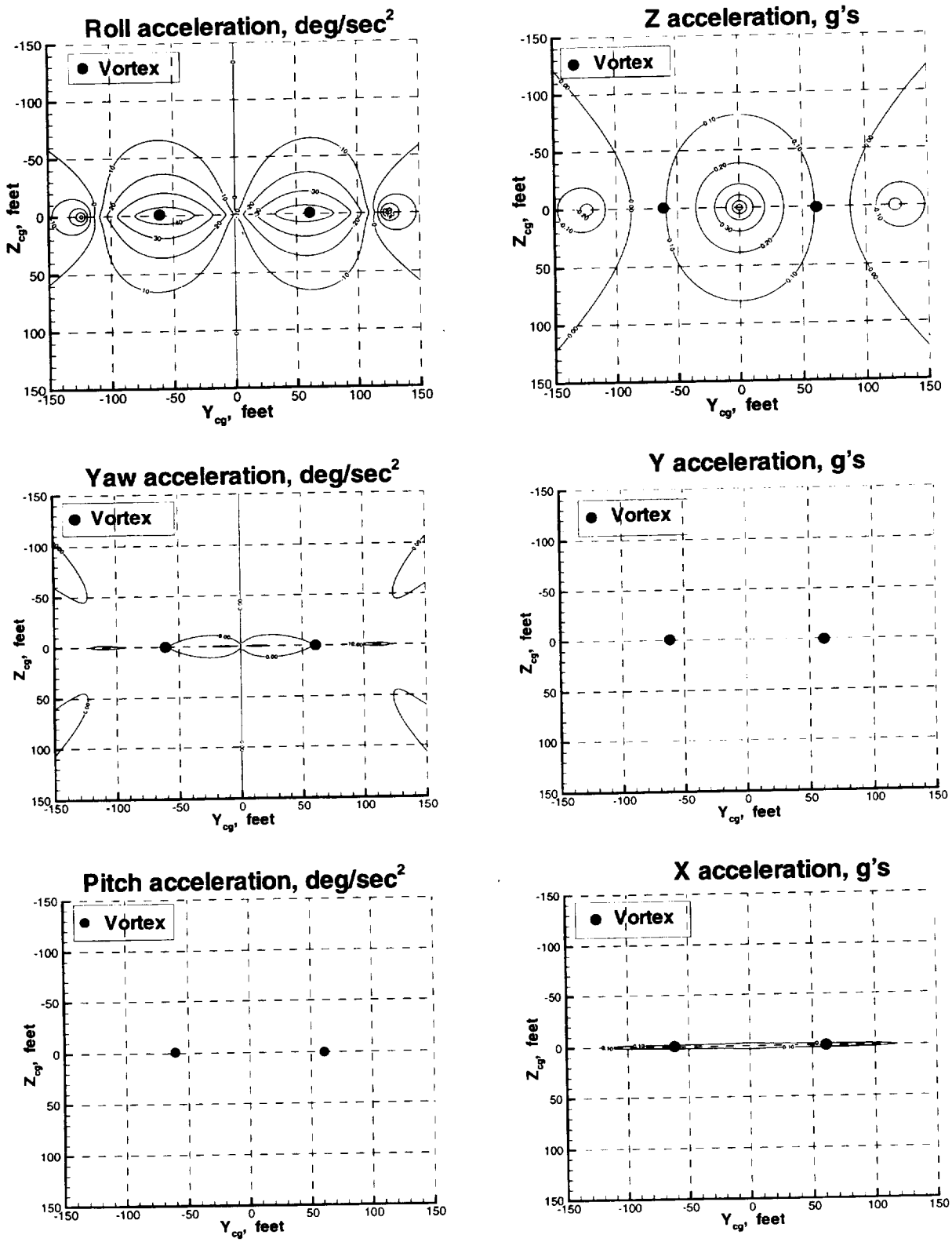

Figure 5. Acceleration contours of rectangular wing in flow field of a vortex pair.

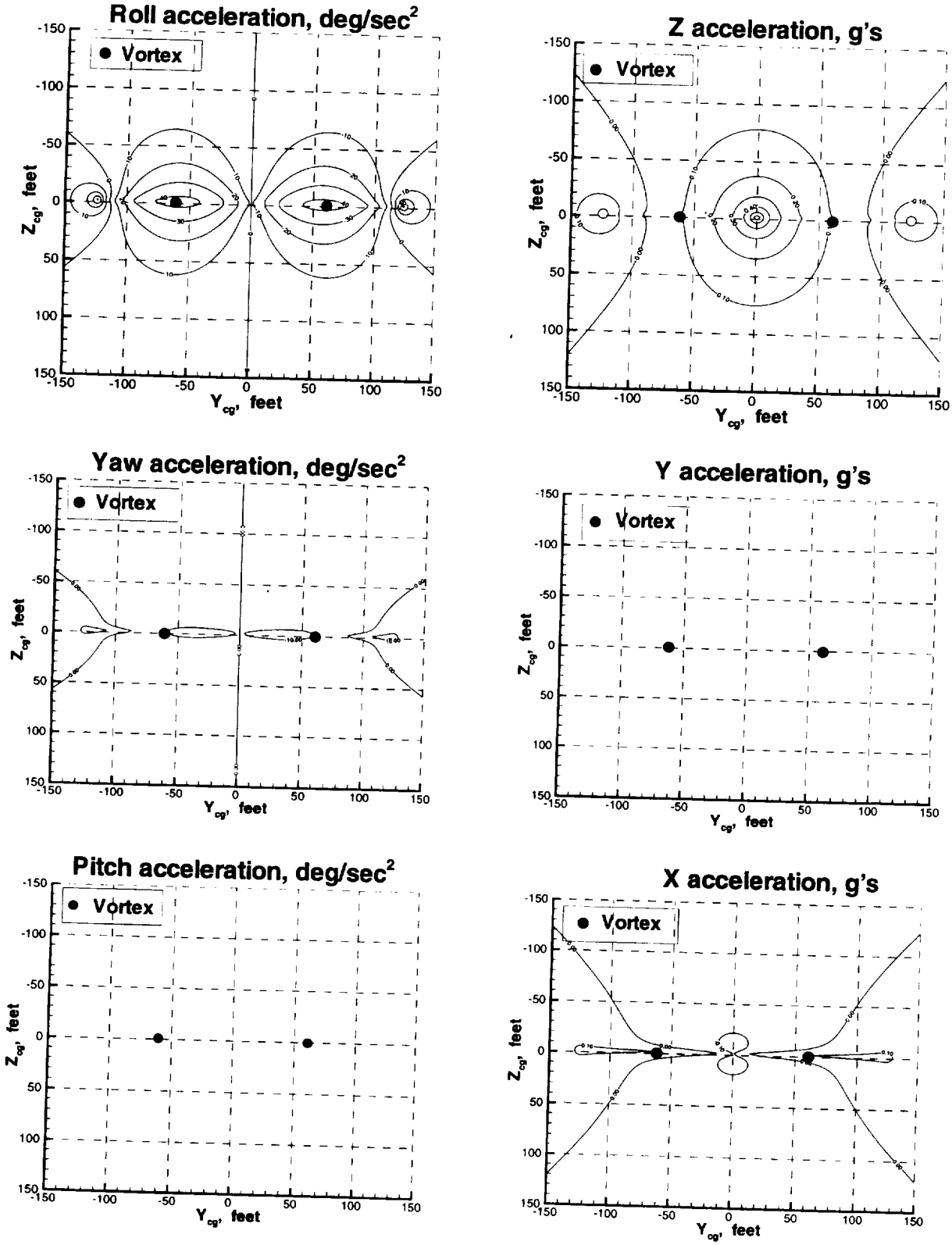

Figure 6. Acceleration contours of rectangular wing with an initial lift coefficient of 1.0 (and angle of attack and pitch attitude of 11.46 degrees).

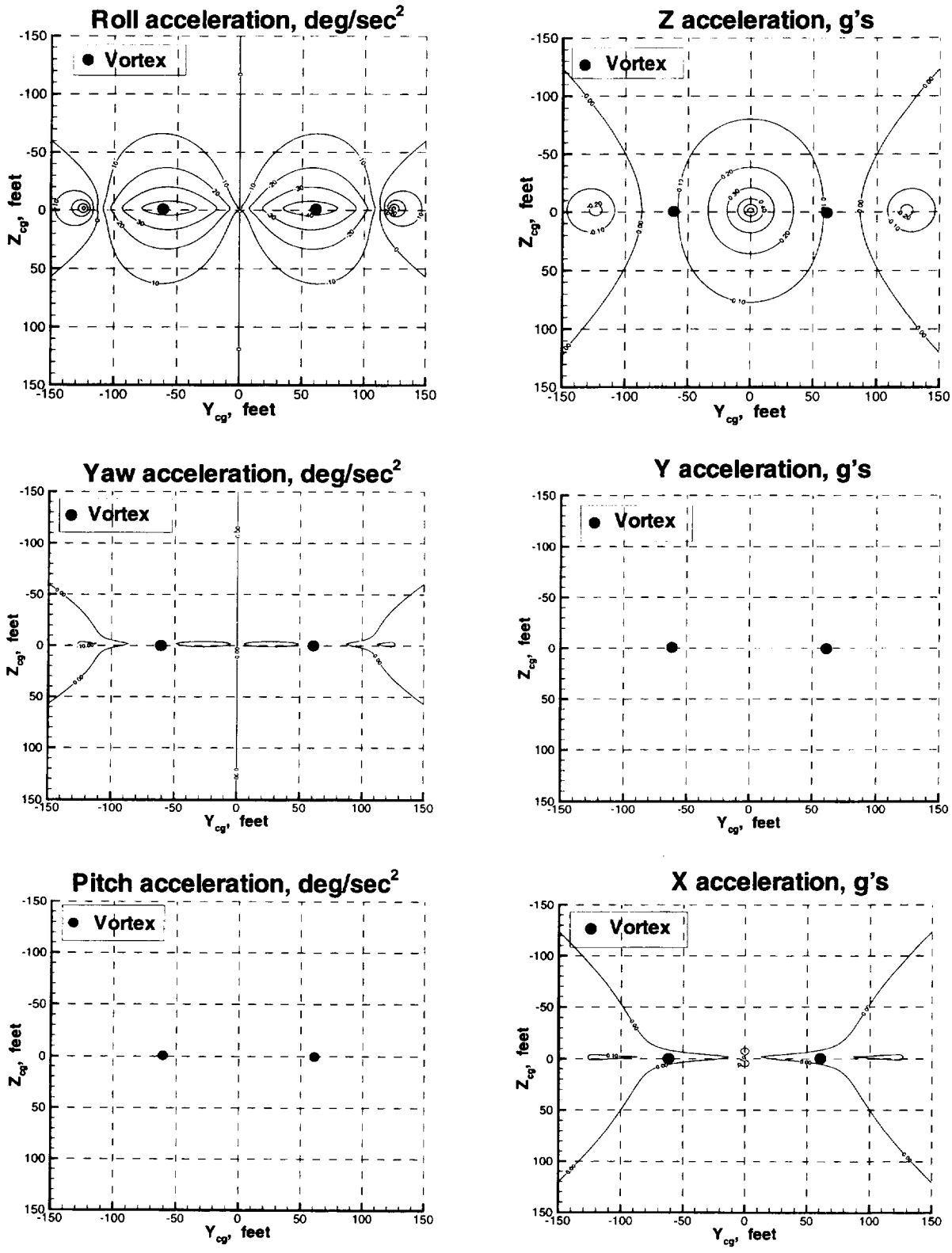

Figure 7. Acceleration contours of a rectangular wing with the effects of drag.

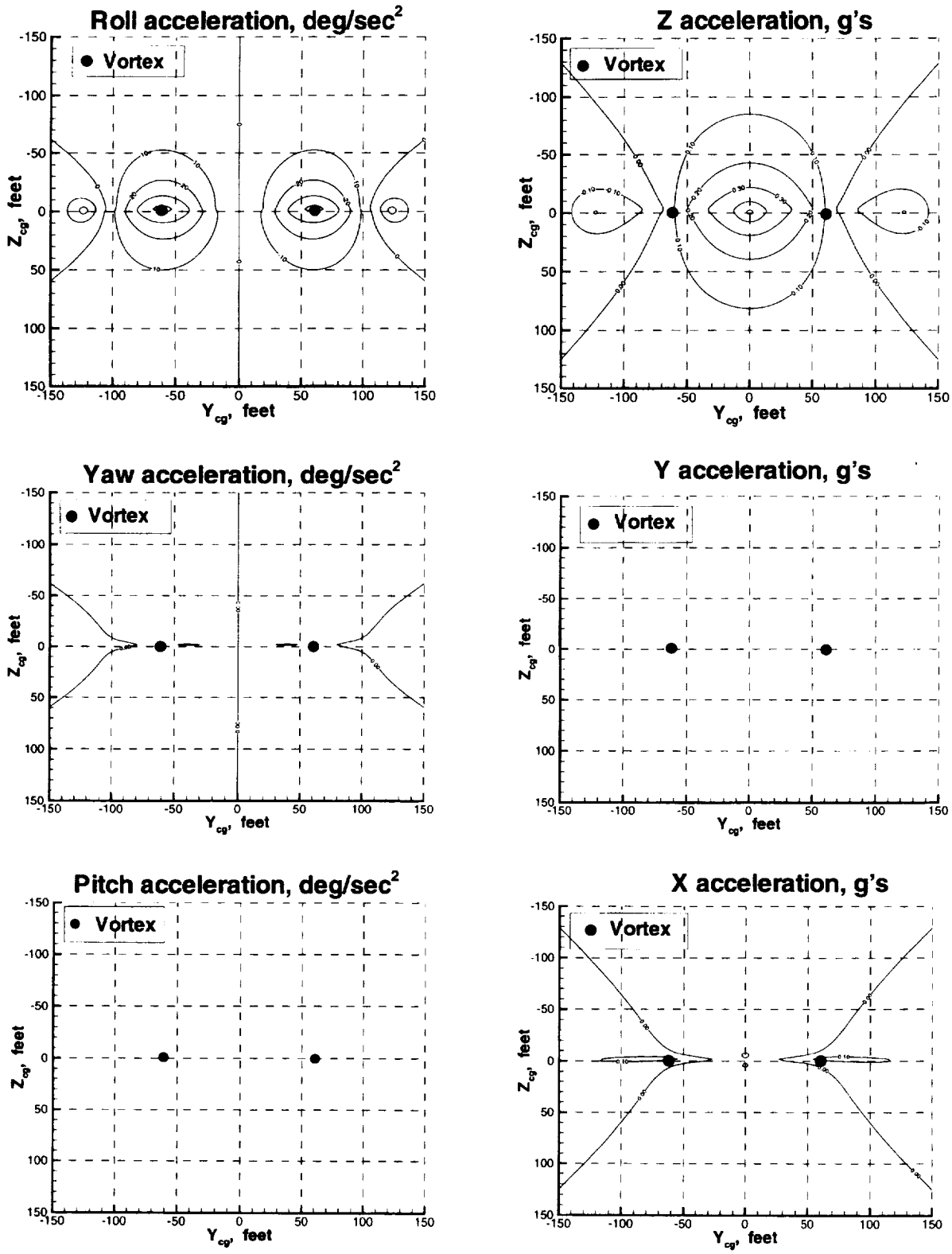

Figure 8. Acceleration contours for wing with a taper ratio of .23.

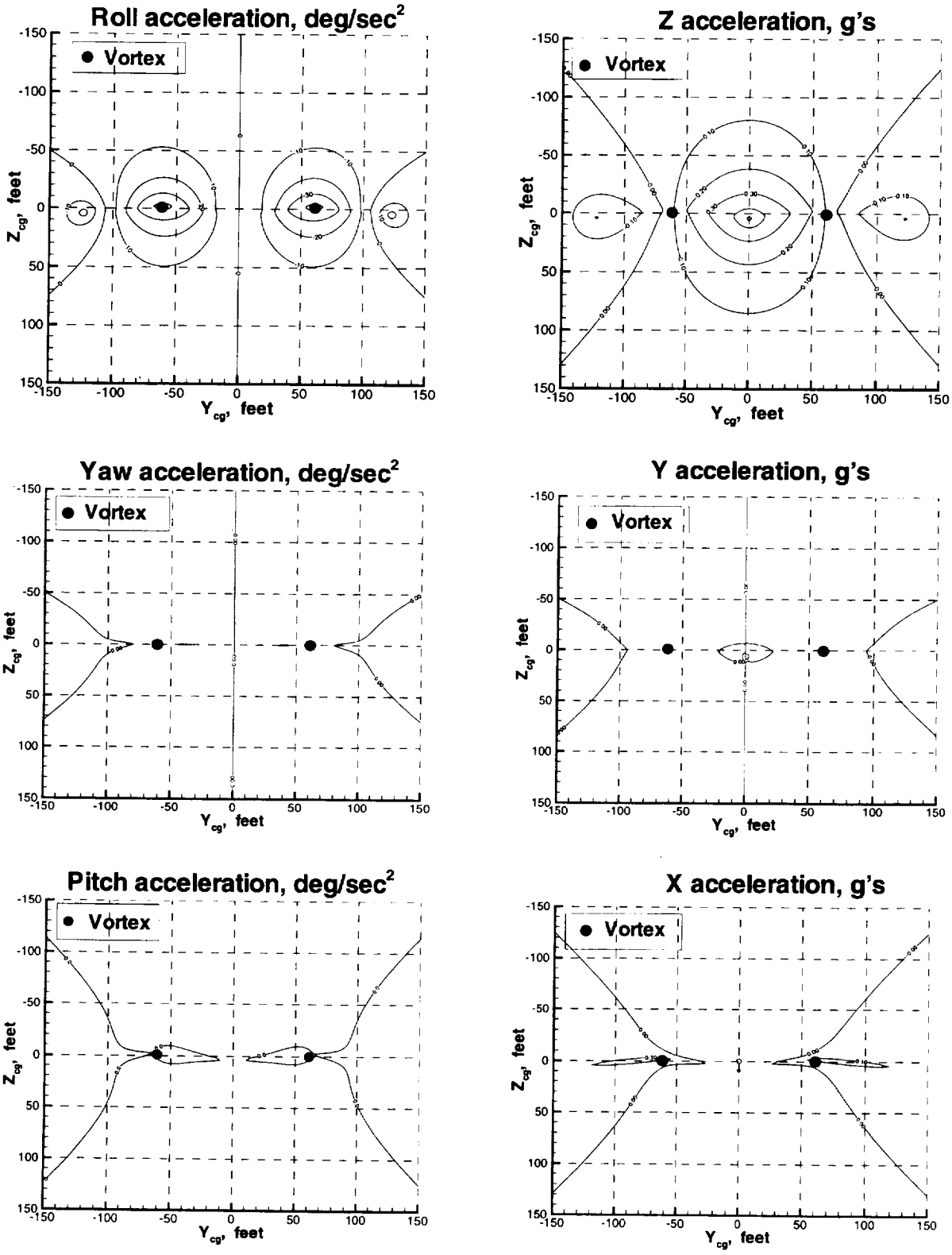

Figure 9. Acceleration contours of wing with a taper ratio of .23 and dihedral of 5 degrees.

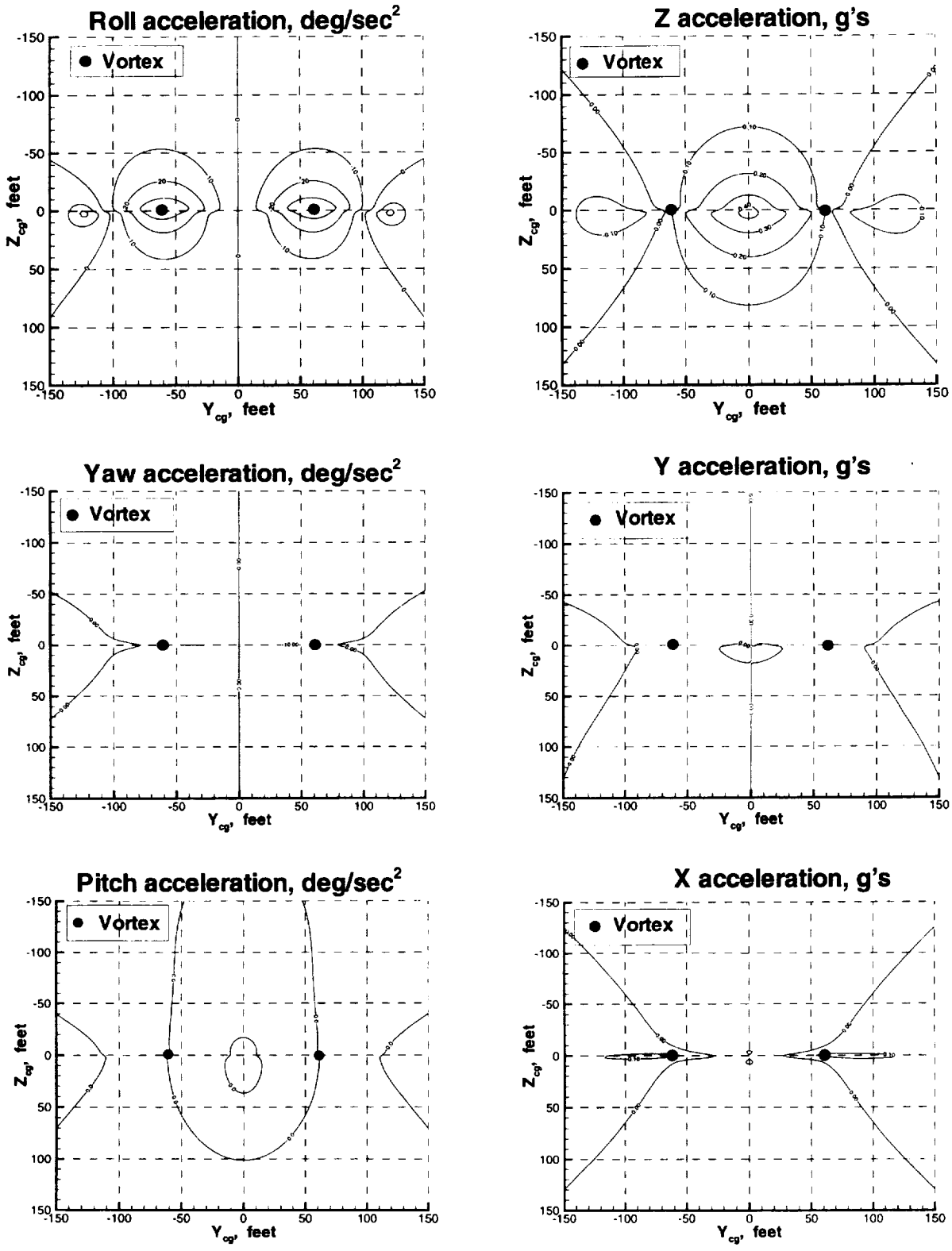

Figure 10. Acceleration contours of wing with a taper ratio of .23, dihedral of 5 degrees, and sweep angle of 25 degrees.

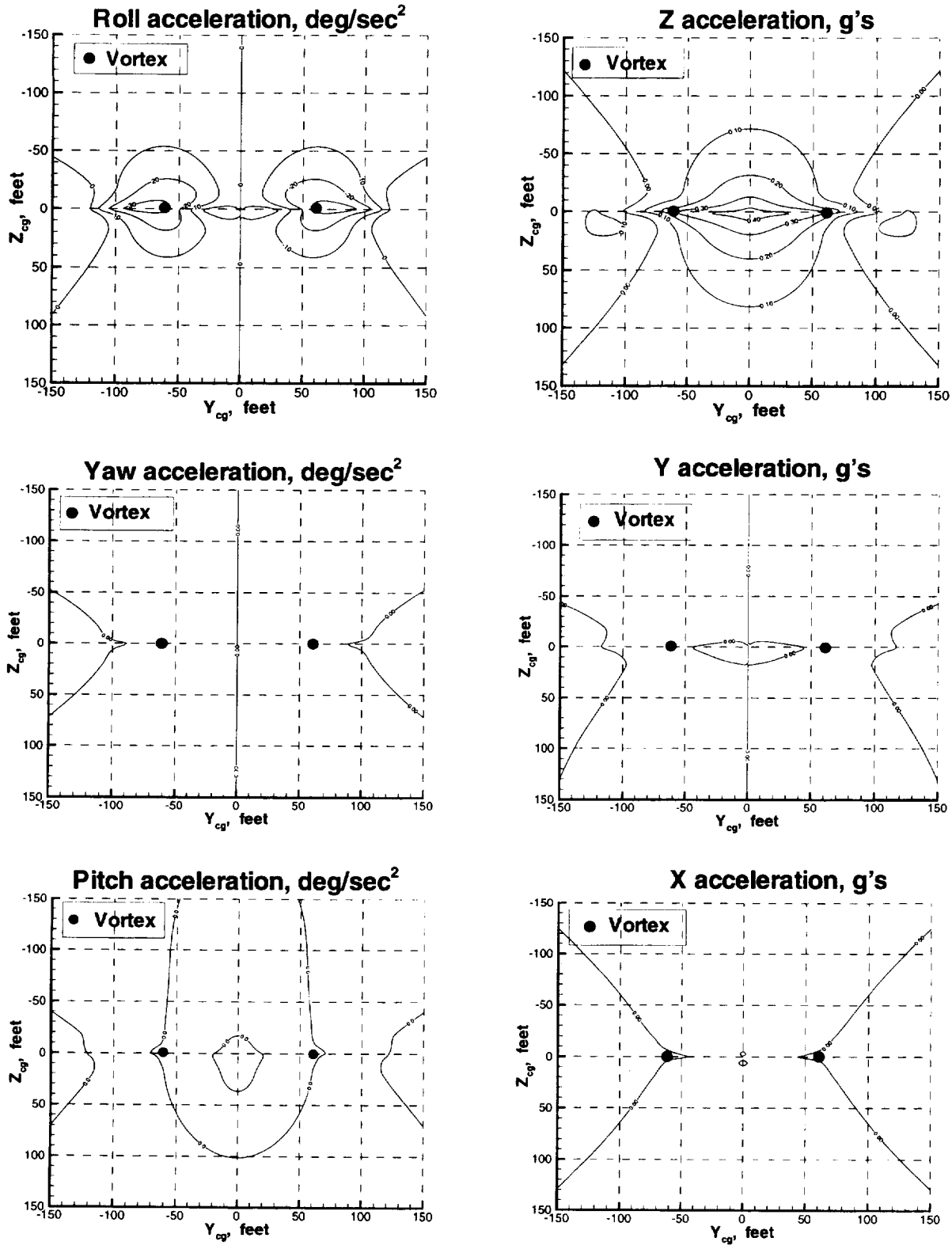

Figure 11. Acceleration contours for complete wing with stall at ±15 degrees angle of attack.

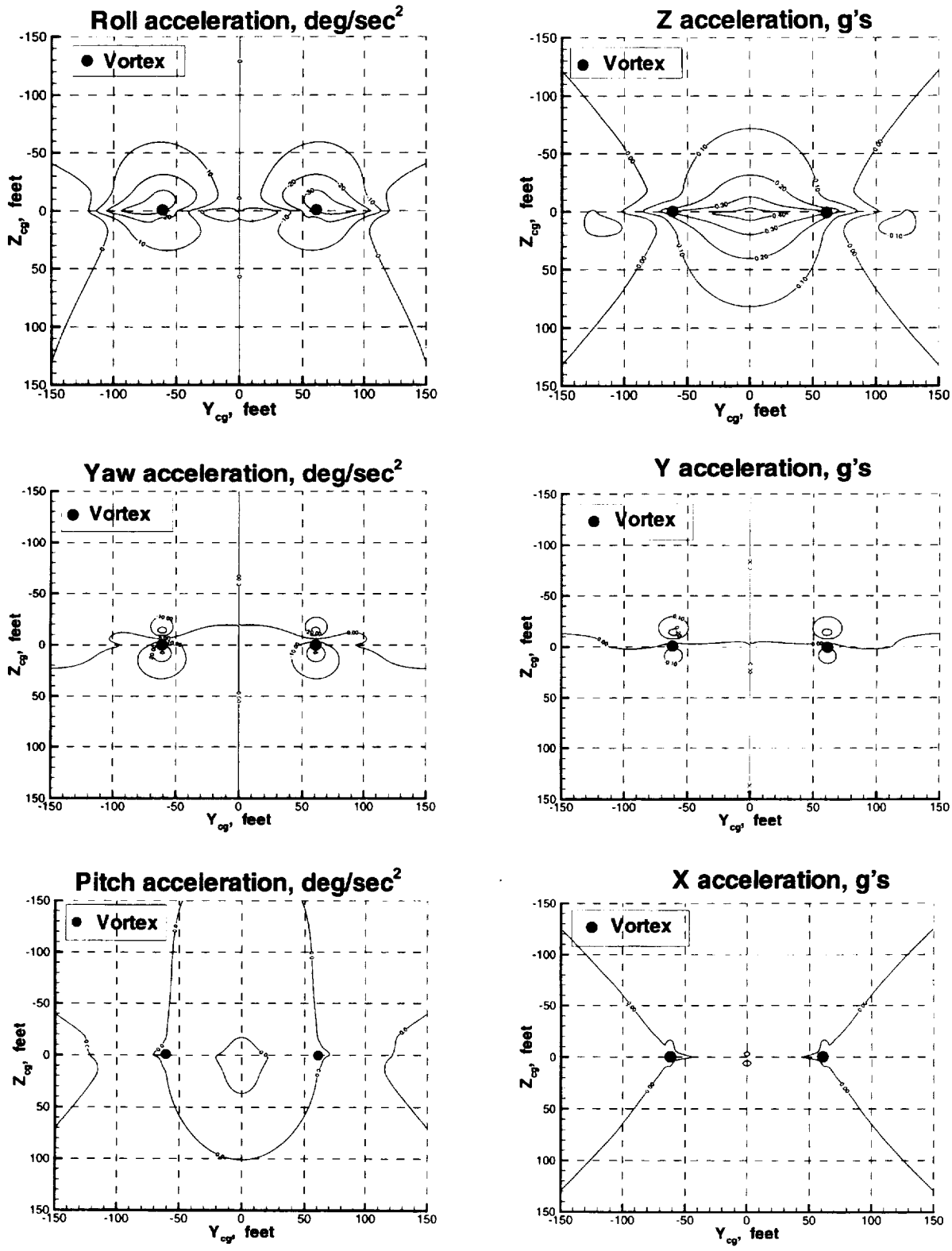

Figure 12. Acceleration contours for complete wing and vertical tail.

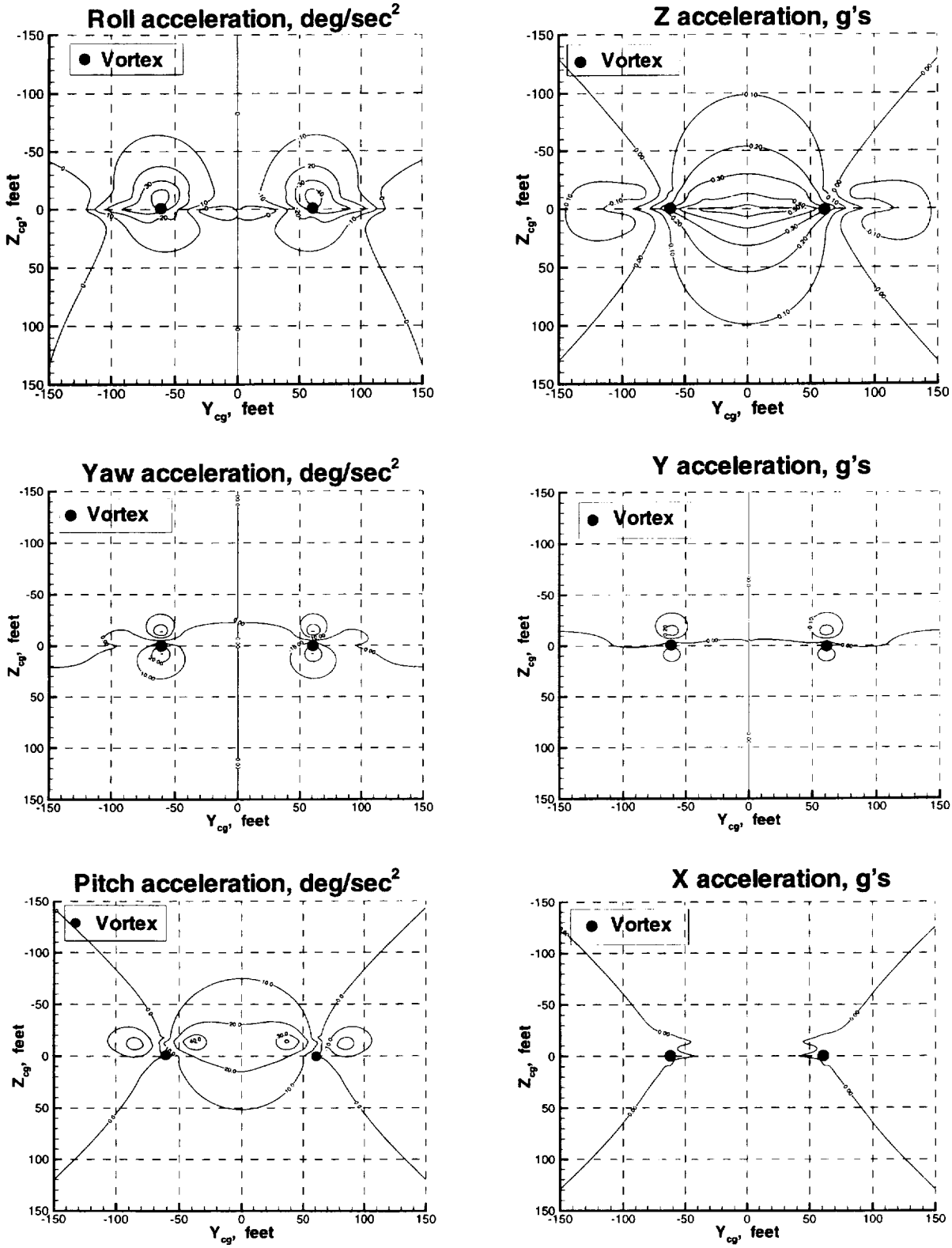

Figure 13. Acceleration contours of a wing, vertical tail, and horizontal tail (complete airplane).

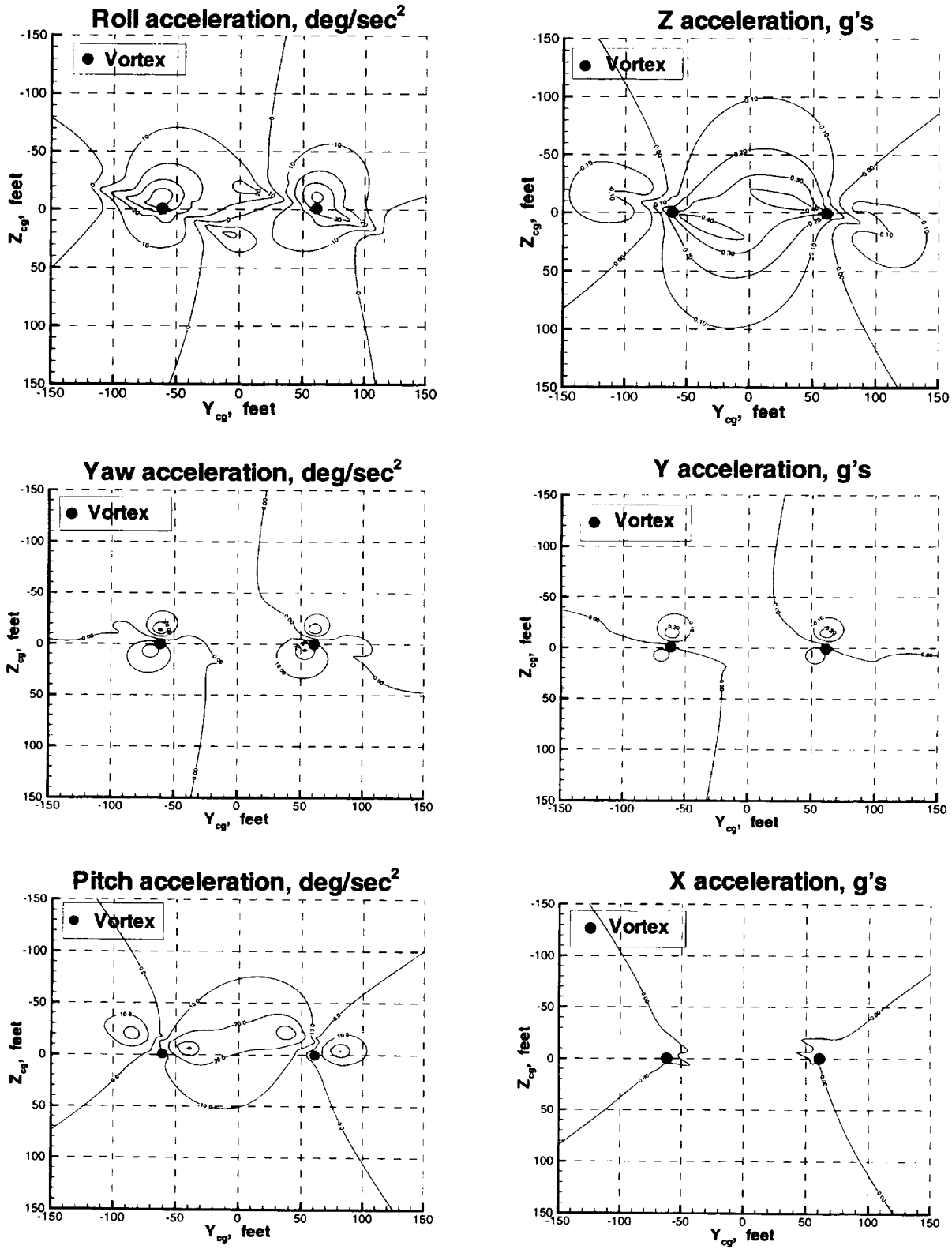

Figure 14. Acceleration contours for complete airplane rolled +20 degrees.

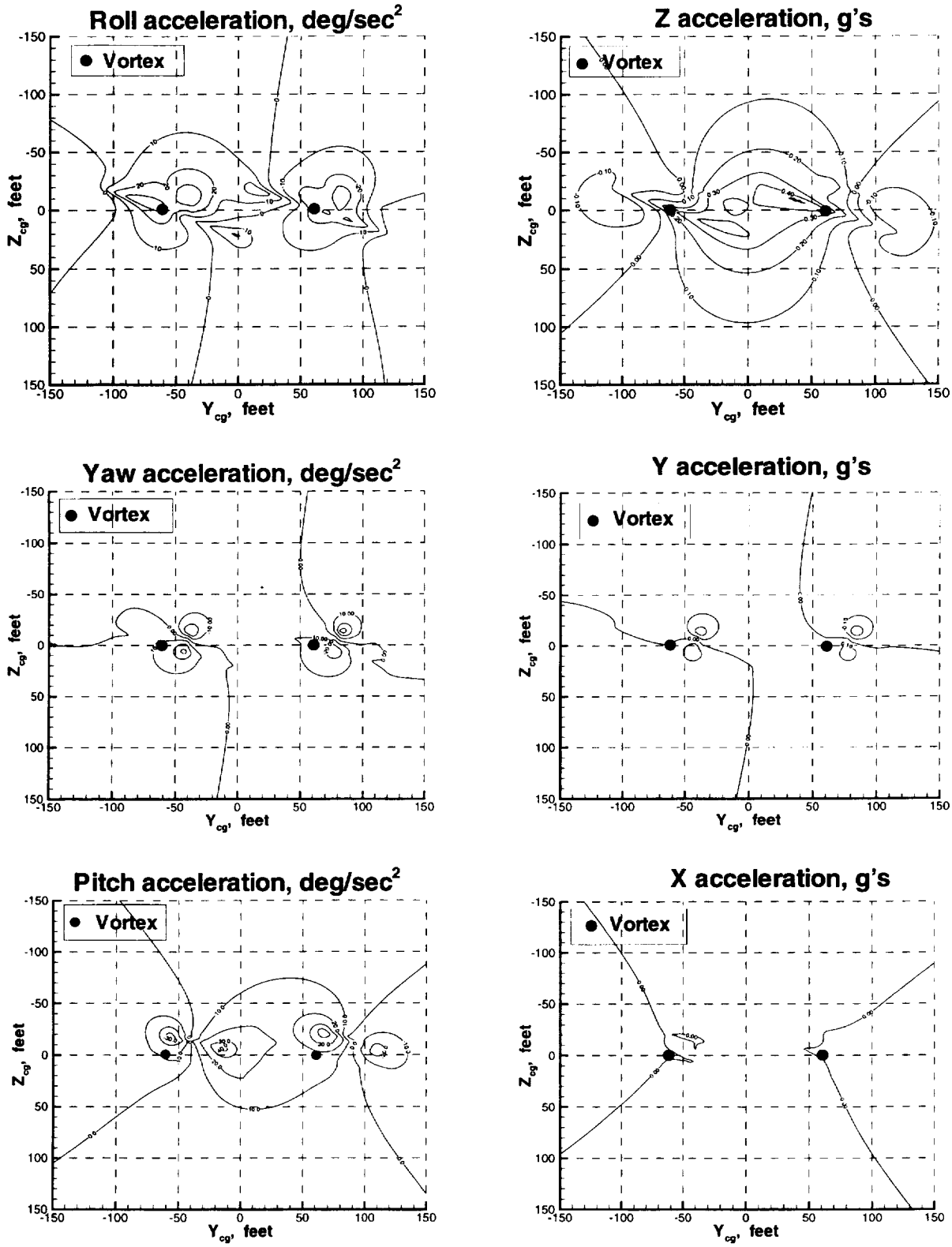

Figure 15. Acceleration contours for complete airplane rolled and yawed +20 degrees.

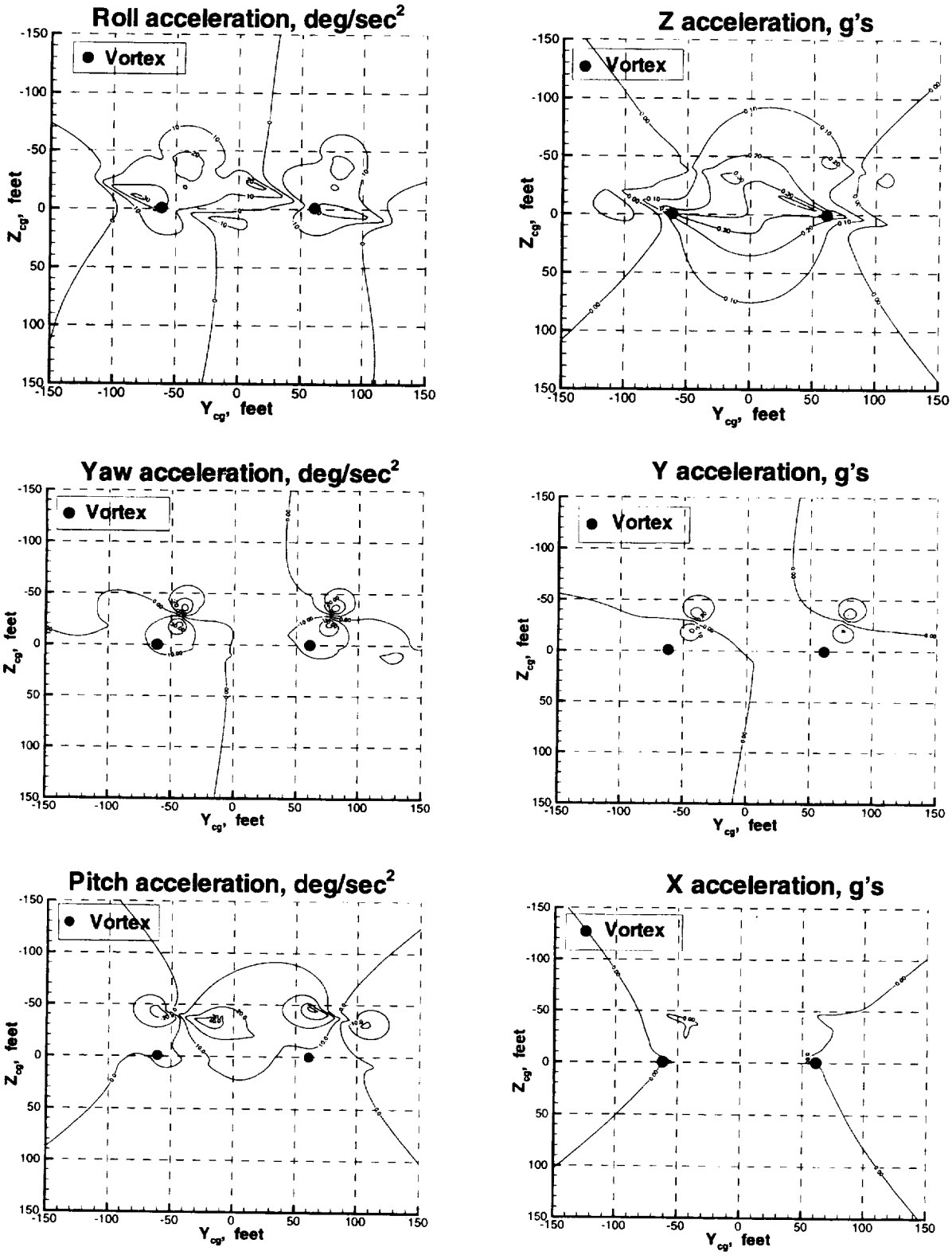

Figure 16. Acceleration contours for complete airplane rolled, yawed, and pitched +20 degrees above nominal attitude.

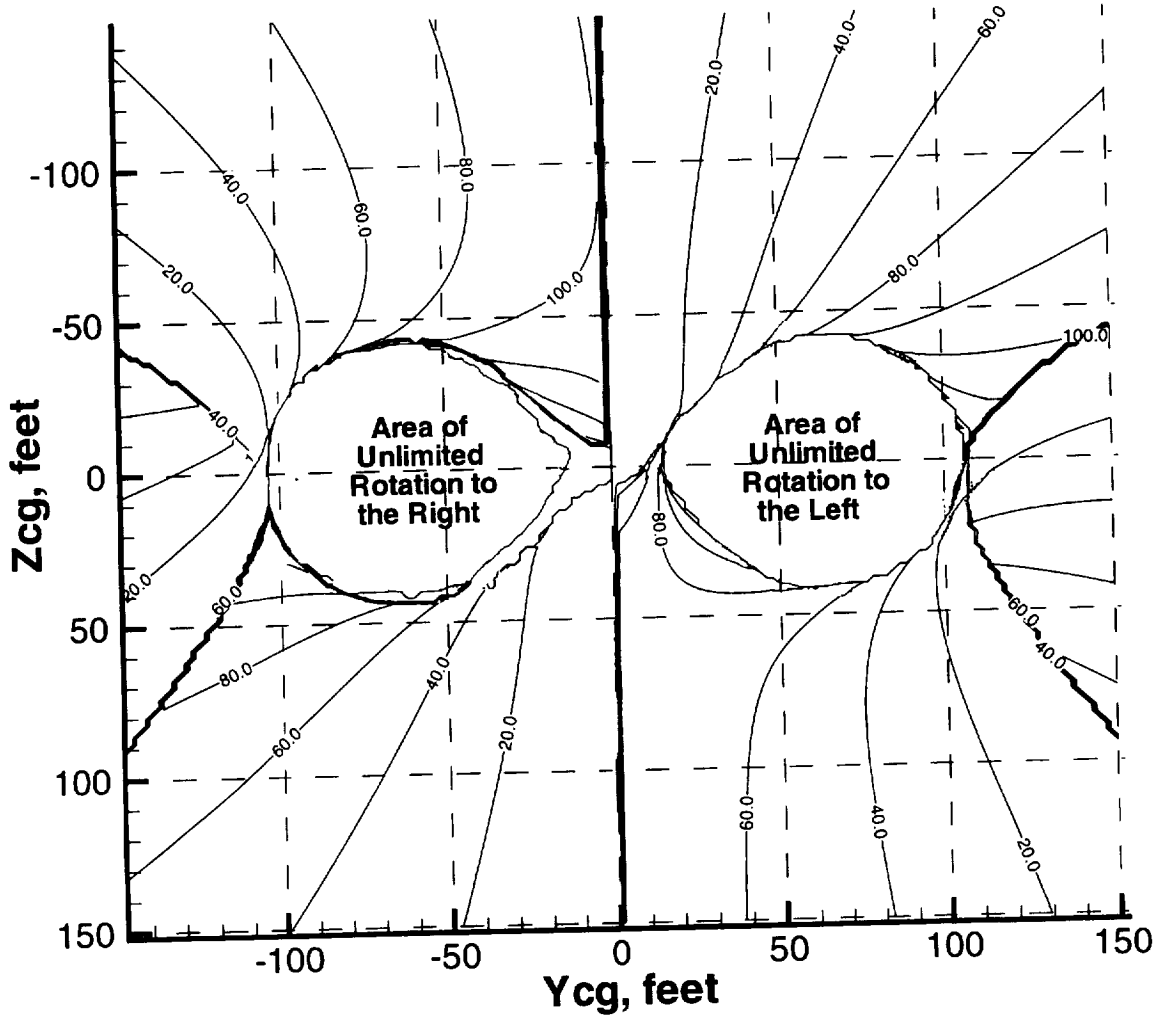

Figure 17. Contours of roll angles that produce zero rolling accelerations for complete airplane.

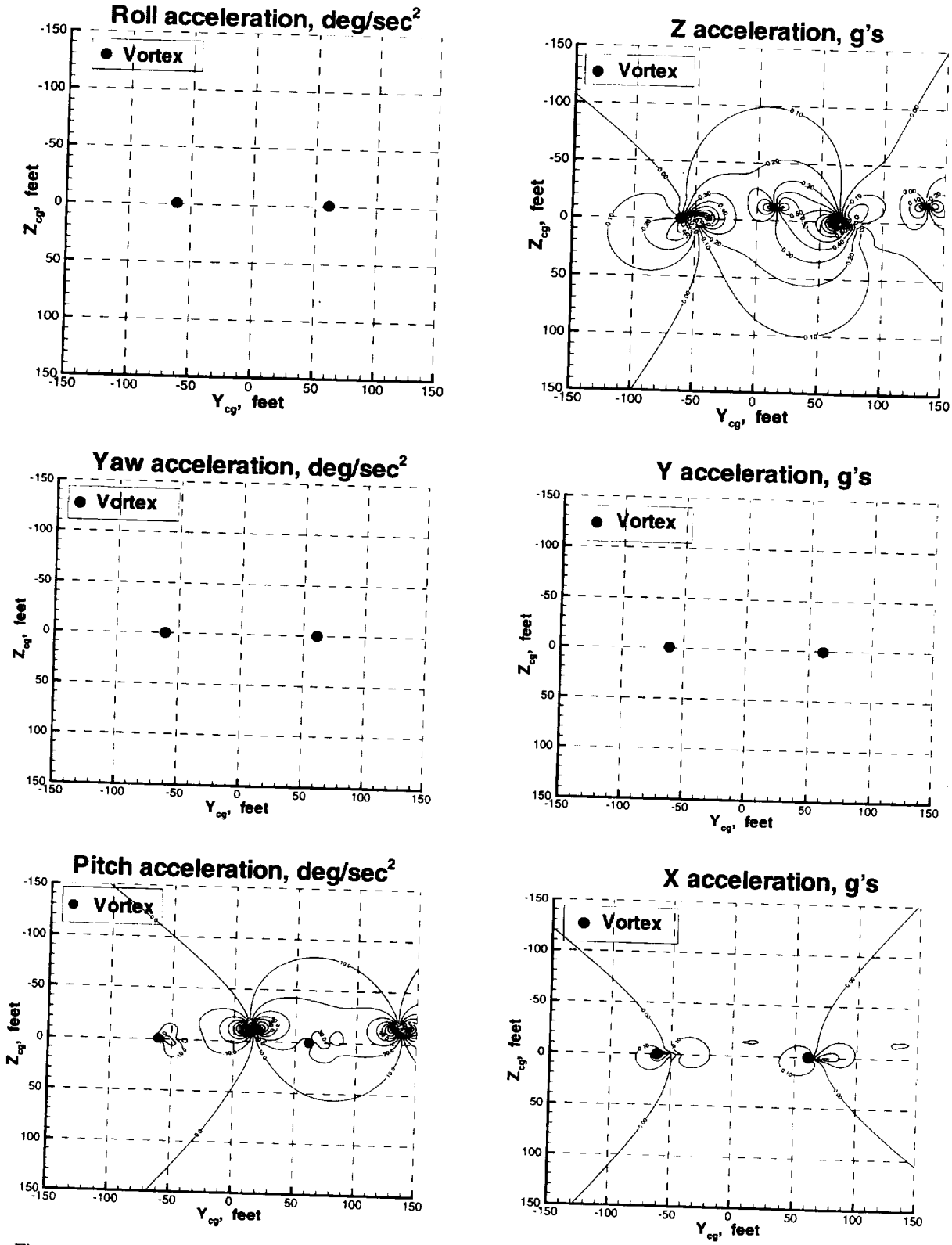

Figure 18. Acceleration contours for complete airplane for a perpendicular encounter (yawed +90 degrees).

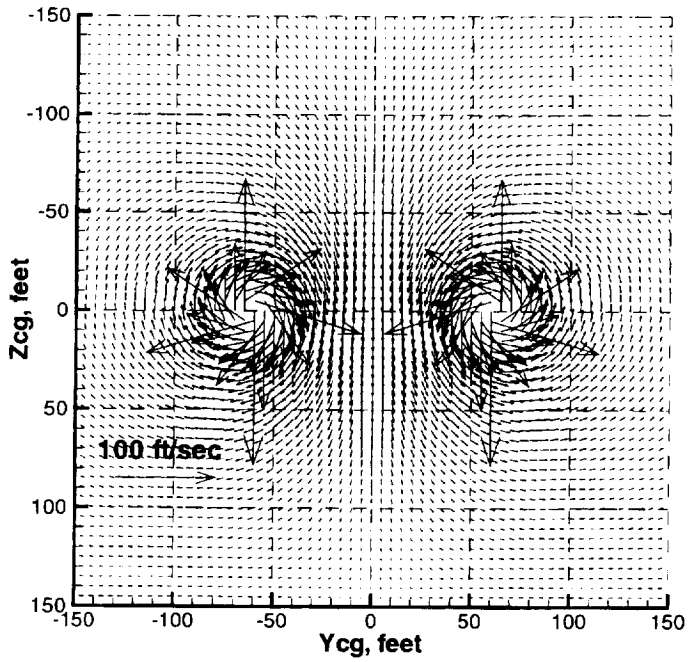

(a) Velocity vector plot.

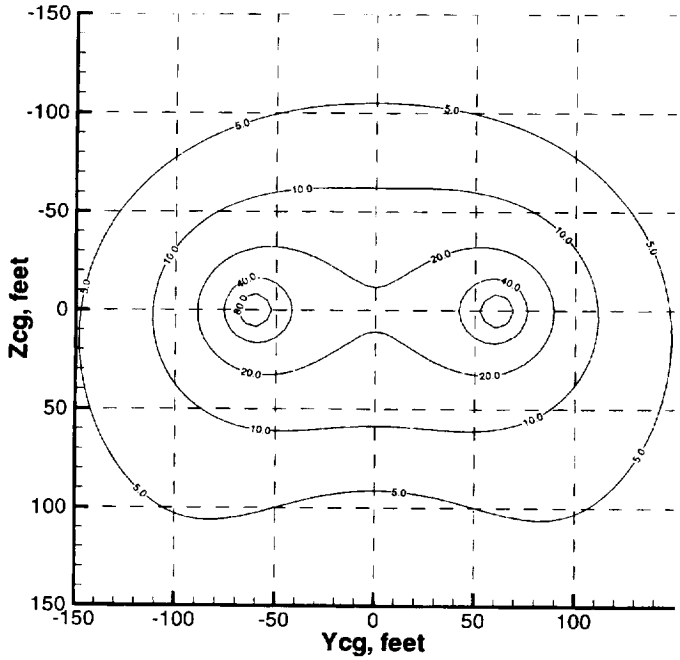

(b) Velocity contour plot.

Figure 19. Flow field for a vortex pair with a ground plane at Z_{cg} = +150 feet (in ground effect 150 feet above ground level).

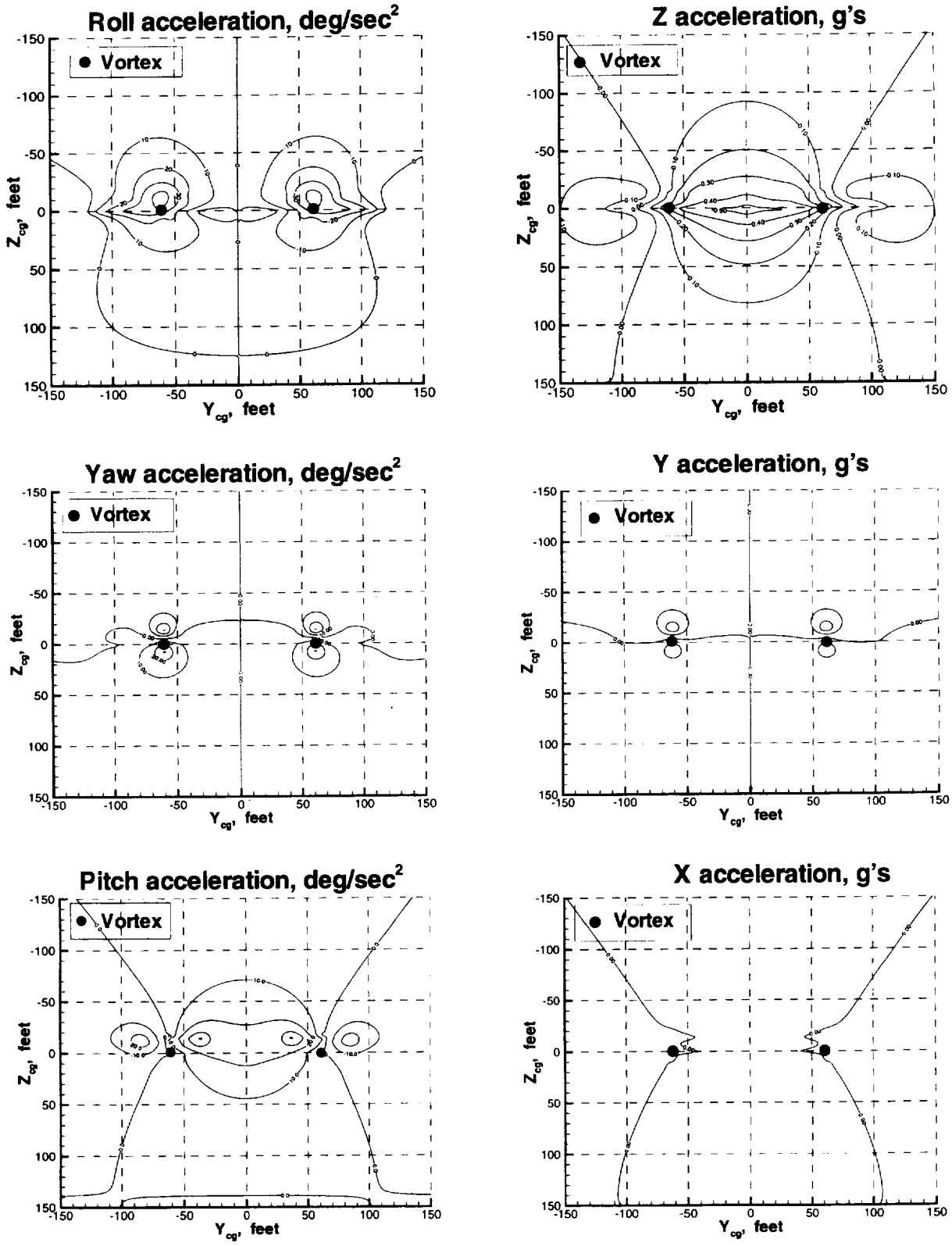

Figure 20. Acceleration contours for complete airplane at nominal attitude in ground effect (vortices 150 feet ground).